Storylines of South Pacific Convergence Zone Changes in a Warmer World

SUGATA NARSEY,[a] JOSEPHINE R. BROWN,[b,c] FRANCOIS DELAGE,[a] GHYSLAINE BOSCHAT,[a,c] MICHAEL GROSE,[d] ROB COLMAN,[a] AND SCOTT POWER[c,e,f]

[a] *Australian Bureau of Meteorology, Melbourne, Victoria, Australia*
[b] *School of Geography, Earth and Atmospheric Sciences, University of Melbourne, Melbourne, Victoria, Australia*
[c] *ARC Centre of Excellence for Climate Extremes, Sydney, New South Wales, Australia*
[d] *CSIRO Oceans and Atmosphere, Hobart, Tasmania, Australia*
[e] *Centre for Applied Climate Sciences, University of Southern Queensland, Toowoomba, Queensland, Australia*
[f] *School of Earth, Atmosphere and Environment, Monash University, Monash, Victoria, Australia*

(Manuscript received 3 June 2021, in final form 19 May 2022)

ABSTRACT: The South Pacific convergence zone (SPCZ) is evaluated in simulations of historical climate from phase 5 of the Coupled Model Intercomparison Project (CMIP5) and phase 6 (CMIP6) models, showing a modest improvement in the simulation of South Pacific precipitation (spatial pattern and mean bias) in CMIP6 models but little change in the overly zonal position of the SPCZ compared with CMIP5 models. A set of models that simulate a reasonable SPCZ are selected from both ensembles, and future projections under high emissions (RCP8.5 and SSP5–8.5) scenarios are examined. The multimodel mean projected change in SPCZ precipitation and position is small, but this multimodel mean response obscures a wide range of future projections from individual models. To investigate the full range of future projections a storyline approach is adopted, focusing on groups of models that simulate a northward-shifted SPCZ, a southward-shifted SPCZ, or little change in SPCZ position. The northward-shifted SPCZ group also exhibit large increases in precipitation in the equatorial Pacific, while the southward-shifted SPCZ group exhibit smaller increases in equatorial precipitation but greater increases within the SPCZ region. A moisture budget decomposition confirms the findings of previous studies: that changes in the mean circulation dynamics are the primary source of uncertainty for projected changes in precipitation in the SPCZ region. While uncertainty remains in SPCZ projections, partly due to uncertain patterns of sea surface temperature change and systematic coupled model biases, it may be worthwhile to consider the range of plausible SPCZ projections captured by this storyline approach for adaptation and planning in the South Pacific region.

SIGNIFICANCE STATEMENT: The South Pacific convergence zone is a band of intense rainfall that influences the weather and climate of many Pacific Island communities. Future changes in the SPCZ will therefore impact these communities. We examine climate model representations of future climate to find out how the SPCZ might change in a warmer world. While the models disagree on future changes in the SPCZ, we suggest that it may be useful to consider groups of models with common "storylines" of future change. The changes in the position of the SPCZ in a warmer world correlate strongly to the amount of rainfall change locally. Some models suggest a northward movement of the SPCZ, while others suggest a southward movement. Consideration of the full range of possible future behavior of the SPCZ is needed to better prepare for the impacts of a warmer climate.

KEYWORDS: South Pacific convergence zone; Climate change; Coupled models; Model evaluation/performance

1. Introduction

The South Pacific convergence zone (SPCZ) is a band of intense precipitation, low-level wind convergence, and active convection that stretches from the equatorial west Pacific to the southeast Pacific (Vincent 1994; Brown et al. 2020; Widlansky et al. 2011). The SPCZ is most active in the austral summer months, and strongly influences the climate of South Pacific islands and surrounding regions. Variability in the position and intensity of the SPCZ occurs on interannual and decadal time scales (e.g., Kiladis et al. 1989; Vincent 1994; Folland et al. 2002; Vincent et al. 2011; Cai et al. 2012), altering precipitation and atmospheric circulation and influencing regions of tropical cyclone genesis (Jourdain et al. 2011; Vincent et al. 2011; Menkes et al. 2012). In some years with very strong El Niño events (e.g., 1982/83 and 1997/98), the SPCZ shifts toward the equator and becomes near zonal, merging with the intertropical convergence zone (ITCZ) into a single convergence zone during so-called "zonal SPCZ" events (Vincent et al. 2011; Cai et al. 2012; Chung and Power 2016; Chung and Power 2015).

Changes in the location, intensity, variability, or existence of the SPCZ may also occur due to anthropogenic global warming. Because the SPCZ is a band of intense rainfall, such a change would profoundly affect the rainfall climate of Pacific Islands within or adjacent to the SPCZ. However, projected

Denotes content that is immediately available upon publication as open access.

Supplemental information related to this paper is available at the Journals Online website: https://doi.org/10.1175/JCLI-D-21-0433.s1.

Corresponding author: Sugata Narsey, Sugata.Narsey@bom.gov.au

DOI: 10.1175/JCLI-D-21-0433.1

changes to the SPCZ in a warmer climate are not well constrained, with no consistent shift in SPCZ position for phase 3 of the Coupled Model Intercomparison Project (CMIP3; Meehl et al. 2007) models (Brown et al. 2012) and phase 5 of the Coupled Model Intercomparison Project (CMIP5; Taylor et al. 2012) models (Brown et al. 2013). Despite these inconsistencies, however, these studies identified a robust drying of the eastern edge of the SPCZ, and a robust tendency for a more northward-shifted SPCZ during El Niño events in a warmer climate. Changes in SPCZ intensity and location may depend on competing thermodynamic and dynamic mechanisms, with decreases in SPCZ precipitation predicted for moderate levels warming, while higher levels of warming may lead to increases in precipitation (Widlansky et al. 2013).

The ability of climate models to simulate the SPCZ, and produce reliable projections of its change, is limited by systematic biases in the tropical Pacific including the "cold tongue" and "double ITCZ" biases (e.g., Christensen et al. 2013). Regional biases in sea surface temperatures (SSTs) and SST gradients are likely to be the cause of the overly zonal orientation of the SPCZ (e.g., Brown et al. 2011; Brown et al. 2013; Niznik et al. 2015). These SST patterns are themselves likely influenced by factors including topographic effects (e.g., Takahashi and Battisti 2007). CMIP3 and CMIP5 models with a worse double ITCZ bias tended to exhibit weaker global mean surface warming with increasing greenhouse gas concentrations (i.e., they have lower climate sensitivity, see Tian 2015). It may therefore be useful to test whether SPCZ changes and climate sensitivity might also be related, since they both appear to be sensitive to tropical Pacific SST pattern effects.

Studies have attempted to address the influence of model biases on climate projections using a range of methods, including bias correction of SSTs as input to dynamical downscaling (e.g., Nguyen et al. 2012; Evans et al. 2016; Dutheil et al. 2019). As the new generation of CMIP6 climate models (Eyring et al. 2016) have an improved simulation of some aspects of the tropical Pacific climate including a reduced "cold tongue" bias (e.g., Grose et al. 2020), they may produce a more realistic simulation of the SPCZ, increasing confidence in future SPCZ projections. However, some degree of uncertainty in future changes to the SPCZ is likely to remain, with diverging future pathways of physical change remaining possible due to uncertainty in future emissions and model uncertainty (e.g., Hawkins and Sutton 2009; Hawkins and Sutton 2011). In the present study we will therefore adopt the approach of Shepherd et al. (2018), attempting to characterize the diverging future pathways of SPCZ changes as distinct "storylines." These storylines will explore the range of plausible changes to the SPCZ with global warming, exploring model-to-model differences. By clarifying the plausibility of these diverging futures in the present study, next-users of climate change projections can simplify their applications to a more limited set of internally consistent physical-change narratives, rather than contending with the full ensemble of climate models and their simulations. Some examples of useful applications might include stress-testing future water resource systems, or adaptation options for species habitats.

The aim of the present study is twofold. First, we evaluate the SPCZ in available CMIP5 and CMIP6 models, and identify those models suitable for further use in our regional projections analyses. We then identify distinct storylines of possible future changes to the SPCZ in a warmer climate, and investigate some of the underlying mechanisms leading to those changes.

In section 2, we describe the data and methods used in the present study. In section 3, we evaluate the simulation of the SPCZ in the CMIP5 and CMIP6 climate model ensembles, identifying models appropriate for regional projections of the SPCZ. In section 4, we investigate the diverging projected SPCZ changes in the CMIP5 and CMIP6 ensembles in a warmer future climate, relating the changes in the SPCZ to historical biases, as well as global and regional processes. Finally, in section 5, we summarize and discuss our findings, and make concluding remarks.

2. Data and methods

a. Models

Model data are provided by the World Climate Research Programme's CMIP5 and CMIP6 (Taylor et al. 2012; Eyring et al. 2016) climate models. These models vary in terms of model components and parameterizations, and represent the state-of-the-art approaches to modeling the complex interactions within the climate system. [See Table A1 in the appendix for details of the models (30 from CMIP6 and 36 from CMIP5) used in the present study. Due to the availability of required model variables, the moisture decomposition is conducted for a subset of analyzed models (40 of the 51 eventually selected models, see Table A2).]

To estimate the influence of anthropogenic warming on the SPCZ, we compare 50-yr periods (1950–99, and 2050–99) to distinguish the forced response more clearly from decadal variability, which is notable in this region (e.g., Folland et al. 2002). To examine a strong climate change signal (not because the emissions pathway is more likely than others), we use the first run for each model from two sets of simulations: a historical scenario including known historical changes in atmospheric composition, and a future scenario forced using a high emissions pathway (RCP8.5 in CMIP5 models and SSP5–8.5 in CMIP6 models). We focus on one scenario for simplicity; however, we acknowledge that the SPCZ changes are potentially sensitive to the level of global warming and therefore the scenario chosen, as described in Widlansky et al. (2013). We conduct our analyses for the December–February austral summer season when the SPCZ is strongest, well developed, and has its greatest impacts on the South Pacific region, as done in previous studies (e.g., Vincent et al. 2011; Brown et al. 2013).

b. Observations

The GPCP observation-based precipitation dataset is used as a benchmark for real world precipitation (Adler et al. 2003). Since global precipitation observations are limited to the satellite era, GPCP data only spans the period from 1979

onward, hence a short period is employed for the observed precipitation climatology (1979–2020). The main conclusions of the present study were not affected by using an alternative precipitation dataset, CMAP (not shown) (Xie and Arkin 1997). The HadISST observation based SST dataset is used as a benchmark for real world SST (Rayner et al. 2003). HadISST data are used here for the period 1950–99.

c. SPCZ line fitting

The SPCZ slope and position are calculated using a simple linear regression method within the domain from 30°S to the equator and from 155° to 220°E following Brown et al. (2011) and Vincent et al. (2011). In this method, the latitude of maximum precipitation is found at each longitude within the domain, and a line-of-best-fit is calculated for those locations.

The diagnosis of SPCZ orientation and location is sensitive to the domain chosen, as well as axis of integration (e.g., searching for longitude of maximum precipitation for each latitude in the domain, not shown here). However, iterating through the longitudinal axis yields a subjectively more sensible fit, perhaps because the SPCZ is more zonal in orientation than it is meridional, especially in models. We also choose here to follow the established method of Brown et al. (2011) and Vincent et al. (2011) for consistency of approach and to facilitate comparison of results presented in this study with previous work.

d. Dynamic-thermodynamic decomposition

To better understand the causes of the projected changes in SPCZ precipitation, we analyze changes in components of the moisture budget between the historical and future scenario experiments, similar to Widlansky et al. (2013). Following Chung et al. (2014), we estimate "thermodynamic" and "dynamic" components of the precipitation changes in each model using a simplified method adapted from Seager et al. (2010) to approximate the moisture budget equation. Chung et al. (2014) define the change ∂ in precipitation P between two states to be

$$\partial P \cong \partial \mathrm{TH} + \partial \mathrm{MCD} + \partial \mathrm{COV} + \partial E, \tag{1}$$

where TH is the thermodynamic contribution to precipitation change, MCD is the contribution due to changes in mean circulation dynamics, COV is related to the covariability of moisture and circulation, and E is evaporation. The quantities ∂P and ∂E are available as model outputs, while ∂TH and ∂MCD are estimated as follows:

$$\partial \mathrm{TH} = \frac{-1}{\rho g}\int_{\mathrm{TOA}}^{p_s} \nabla \cdot (\mathbf{u}_0[\partial q])dp, \tag{2}$$

$$\partial \mathrm{MCD} = \frac{-1}{\rho g}\int_{\mathrm{TOA}}^{p_s} \nabla \cdot (q_0[\partial \mathbf{u}])dp, \tag{3}$$

where ρ is the density of water, g is the acceleration due to gravity, p_s is the surface pressure, TOA is the top of atmosphere, $\mathbf{u}$ is the horizontal wind vector, q is the specific humidity, and the subscript 0 denotes values from the historical period. The thermodynamic component (∂TH) gives the change in precipitation arising from changes in moisture convergence in the absence of circulation changes. The dynamic term (∂MCD) gives the change in precipitation arising from changes in the moisture convergence due to circulation changes, in the absence of changes in the vertical moisture profile. The covarying term (∂COV) represents the contribution of coherent changes in time and space covariability in both moisture and the circulation to long-term average moisture convergence. Here ∂COV is approximated as the difference between precipitation change (∂P) and all the other terms. Although this is not a precise estimate of ∂COV it is a reasonable approximation for the purposes of this study since ∂COV is typically small compared to other terms (∂MCD and ∂TH) and is known to be small in the region of interest here (see Seager et al. 2010, their Fig. 3).

e. Indices

As described above, the SPCZ varies with the El Niño–Southern Oscillation (ENSO). We characterize ENSO variability using December–January–February relative SST in the Niño-3.4 region (5°N–5°S, 170°–120°W). Relative Niño-3.4 SST is calculated as the difference between the SST in the Niño-3.4 region and the mean SST over all tropical oceans (30°S–30°N) for each season. This is similar to the relative Niño-3.4 index of van Oldenborgh et al. (2021); however, one key difference is that our index does not require a defined baseline period, and as such is relevant for changes in both the variability as well as the mean state of tropical Pacific asymmetry (e.g. Ramsay and Sobel 2011; Grose et al. 2014).

Equilibrium climate sensitivity (ECS) is a measure used to gauge each model's global climate response to greenhouse gas concentrations, and is quantified as the change in global mean surface temperature in response to a doubling of atmospheric CO_2 concentration allowing for time to equilibrate, typically 150 years (National Research Council 1979). ECS values for CMIP5 and CMIP6 models computed using the Gregory et al. (2004) method are taken from Tables 1 and 2 of Meehl et al. (2020) and summarized later (Table A2). Note that CMIP6 models indicate a larger range of climate sensitivity, with ECS values spanning 1.8°–5.6°C across models and exceeding 4.5°C in 10 of these models (compared to 2.1°–4.7°C in CMIP5, e.g., Zelinka et al. 2020), leading to a higher warming in the future climate simulations in those models with high climate sensitivity and in the CMIP6 multimodel mean.

Many climate models have an equatorial Pacific cold-tongue bias (Li and Xie 2014), where cold SSTs extend too far westward into the west Pacific warm pool region and influence the regional climate. Here we quantify the cold-tongue bias using a simple cold tongue index (CTI) following Grose et al. (2020): the average model SST bias in the west Pacific warm pool region (155°–175°E, 10°S–10°N), calculated relative to HadISST observations.

3. Model evaluation

a. The SPCZ mean state

The biases in the CMIP5 and CMIP6 multimodel mean SST and precipitation in the tropical Pacific relative to

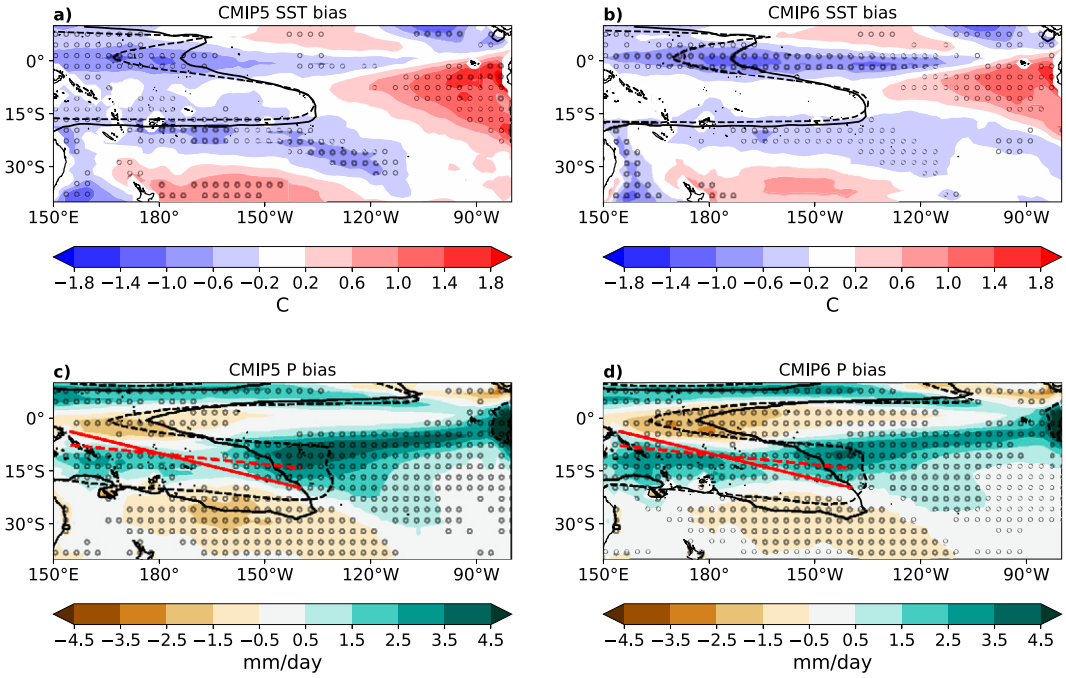

FIG. 1. Multimodel mean biases in SST (°C) relative to HadISST observations for (a) CMIP5 and (b) CMIP6 models and multimodel mean biases in precipitation (mm day^{-1}) relative to GPCP for (c) CMIP5 and (d) CMIP6 models. Temperature biases are for 1950–99, while precipitation biases are for 1979–99. Stippling indicates where greater than two-thirds of models are biased in the same direction. The contours represent the 28°C SST contour in (a) and (b) and the 5 mm day^{-1} contour in (c) and (d) for observations (solid) and the MMM (dashed). The diagnosed SPCZ position (linear fit to maximum precipitation) for observations (solid) and the MMM (dashed) are shown in red.

observations are shown in Fig. 1. The biases in SST (Figs. 1a,b) are known to be important for simulating tropical precipitation, including the SPCZ (e.g., Brown et al. 2013), and are also known to influence future projections of tropical precipitation (e.g., Chadwick et al. 2014; Grose et al. 2014). As noted in other studies (e.g., Grose et al. 2020), some aspects of the biases in tropical Pacific SST in the multimodel mean (MMM) are reduced in the CMIP6 ensemble compared with the CMIP5 ensemble. There is a reduction in the cold bias in the southwest Pacific and the ensemble mean zonal SST gradient in the tropical Pacific is slightly closer to observed. However, the cold tongue bias in the western equatorial Pacific appears to be slightly larger east of the date line in CMIP6 models.

The biases in CMIP5 and CMIP6 MMM seasonal average precipitation and model agreement on bias displayed as stippling (Figs. 1c,d) are similar in the South Pacific, with an overly dry equatorial western Pacific in the region of model cold SST biases. This western equatorial Pacific dry bias is greater in the CMIP6 MMM, consistent with the stronger SST cold bias. There is a reduced bias in the subtropical or diagonal component of the SPCZ in the CMIP6 MMM, evident in a smaller dry bias to the southwest of the SPCZ and a smaller wet bias to the northeast of the SPCZ. The "double ITCZ" in the eastern Pacific persists in the CMIP6 MMM but is reduced in magnitude compared with the CMIP5 MMM. As a result of the mean-state biases in models, both the CMIP5 and CMIP6 MMM have an SPCZ that is too zonal in orientation compared to observations, and even with the improvements in the double ITCZ bias in CMIP6 models, the CMIP6 MMM SPCZ orientation shows no clear improvement compared to the CMIP5 MMM.

Model performance is also evaluated by calculating the spatial (pattern) correlation coefficient and root-mean-square error (RMSE) of precipitation over the SPCZ region (30°S–0°, 155°E–140°W) for all models relative to observations (Figs. 2a,b and Table A1). The spread of correlations and RMSE values for the CMIP5 and CMIP6 ensemble members provides information about the full range of model performance, whereas the MMM bias shown in Fig. 1 does not capture this model range. The improvement in SPCZ-region precipitation from CMIP5 to CMIP6 models is striking, with 75% of CMIP6 models performing better than the median model in the CMIP5 ensemble for spatial correlation and lower RMSE values for the CMIP6 models. The SST climatology spatial correlation with HadISST is only slightly improved in CMIP6 compared to CMIP5, while the RMSE is similar between ensembles (not shown).

The inter-model ranges of slope and position of the SPCZ are quite large (Fig. 2c and Table A1). No individual model produces an SPCZ slope equal to or larger than observed, while there is no systematic bias in the SPCZ position in either CMIP5 or CMIP6 ensembles. However, some outliers in SPCZ position and slope are identified. These models are also found to have a poor spatial correlation with observed precipitation over the SPCZ region, suggesting an especially poor SPCZ

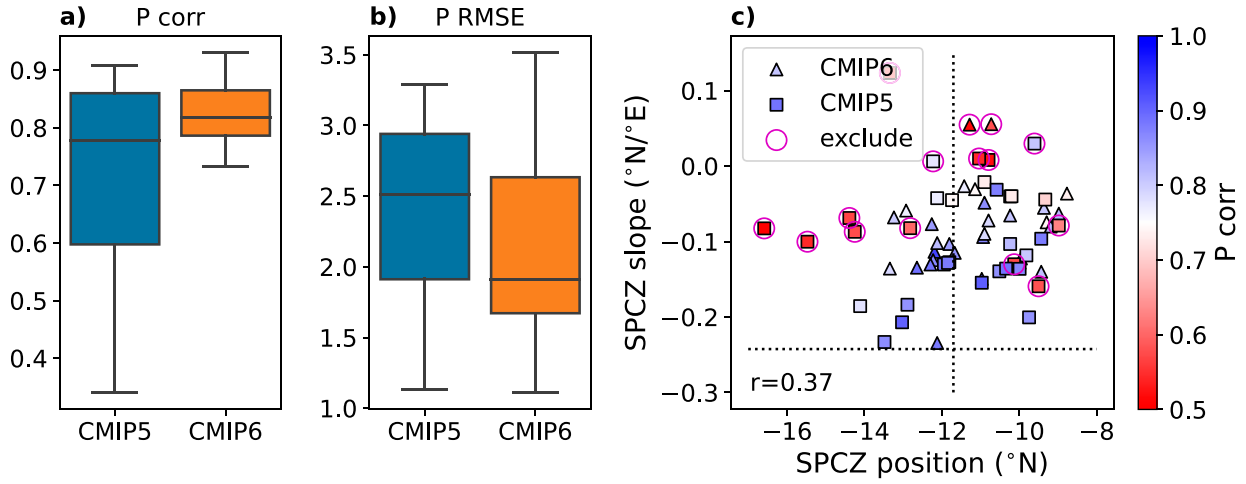

FIG. 2. Historical SPCZ precipitation climatology (a) spatial pattern correlation, (b) RMSE (mm day^{-1}), and (c) diagnosed SPCZ position vs slope in each model, compared against GPCP observations (dotted line) for CMIP5 and CMIP6 models. All calculations are for the SPCZ region (30°S–0°, 155°E–140°W). Shading in (c) represents each model's spatial pattern correlation. Circled models are excluded based on poor simulation of SPCZ (see text for details). Correlation (r) between SPCZ position and slope is given in (c) for the non-excluded models.

simulation, although this may be linked to a failure of our method to accurately separate the SPCZ from regional biases (e.g., eastern Pacific double ITCZ). Attempts to modify the identification scheme, or the domain used, did not subjectively improve the identification of the SPCZ in those models (not shown). Poor identification of the SPCZ appears to be related to the strength of the eastern Pacific double ITCZ in some models (Figs. S1 and S2 in the online supplemental material).

To investigate future projections of the SPCZ, we therefore subset the CMIP5 and CMIP6 ensembles to include only those models that we deem able to simulate the SPCZ, or where our diagnostic can identify the model SPCZ. We define an inadequately simulated SPCZ as follows. For all following analyses, we exclude any model in which the diagnosed SPCZ is oriented from the southwest to the northeast (i.e., has a slope $> 0°$), a mean SPCZ position south of 15°S, or a spatial correlation coefficient of precipitation pattern against observations of less than 0.65. Of the 15 models excluded, 13 are from the CMIP5 ensemble.

b. *Variability of the SPCZ*

In observations, the SPCZ varies on time scales ranging from days to decades (Brown et al. 2020). Here we evaluate a well-documented feature of the observed SPCZ—how its position varies with ENSO on interannual time scales. We consider how the identified position of the SPCZ varies with the relative Niño-3.4 index, comparing the relationship in models with observations (Figs. S3 and S4). We find that there is no obvious improvement in the relationship between SPCZ position and relative Niño-3.4 index in the CMIP6 ensemble compared to CMIP5.

4. Projected changes to the SPCZ

a. *CMIP5 and CMIP6 projected SPCZ changes*

The multimodel mean projected changes in surface temperature (relative to the tropical mean SST change) and precipitation are shown for both CMIP5 and CMIP6 ensembles (Fig. 3). The SPCZ region warms less than the tropical mean SST in both ensembles. The pattern of absolute precipitation change in CMIP6 MMM is similar to CMIP5 MMM, and the strong increase in equatorial precipitation is similar. However, the drying on the eastern edge of the SPCZ is stronger, and there is a slight increase in degree of model agreement on the sign of precipitation change in the western SPCZ region, in CMIP6 models compared with CMIP5 models. One interesting development is the reduced precipitation change in the west Pacific warm pool (e.g., 150°E–180° near the equator) in the CMIP6 ensemble compared to CMIP5. This is surprising since west Pacific precipitation changes appeared to be related to SST biases in CMIP5 models (Brown et al. 2013), and the SST and precipitation biases in that region are slightly larger on average in the CMIP6 historical simulations compared to CMIP5 (see Fig. 1).

The MMM precipitation changes in the SPCZ region are small in both the CMIP5 and CMIP6 cases, masking large contrasts between individual models in their future projections of SPCZ precipitation (Figs. S5 and S6). Similarly, the diagnosed SPCZ slope and position in both the CMIP5 and CMIP6 MMMs does not change markedly between historical and future climates (Figs. 3c,d and Table A2). As we will describe below, this reflects a cancellation between opposing changes in the SPCZ found in individual models in each ensemble.

The model spread in changes in SPCZ position and orientation are correlated ($r = 0.71$), with equatorward shifts in the SPCZ being accompanied by a zonal change in the SPCZ orientation in individual models, and vice versa (Fig. 4a). There is no clear indication from the two ensembles on the direction of SPCZ changes, with a similar number of models predicting equatorward and poleward shifts in the SPCZ.

How do the changes in the diagnosed SPCZ position and slope relate to projected precipitation changes in the Pacific

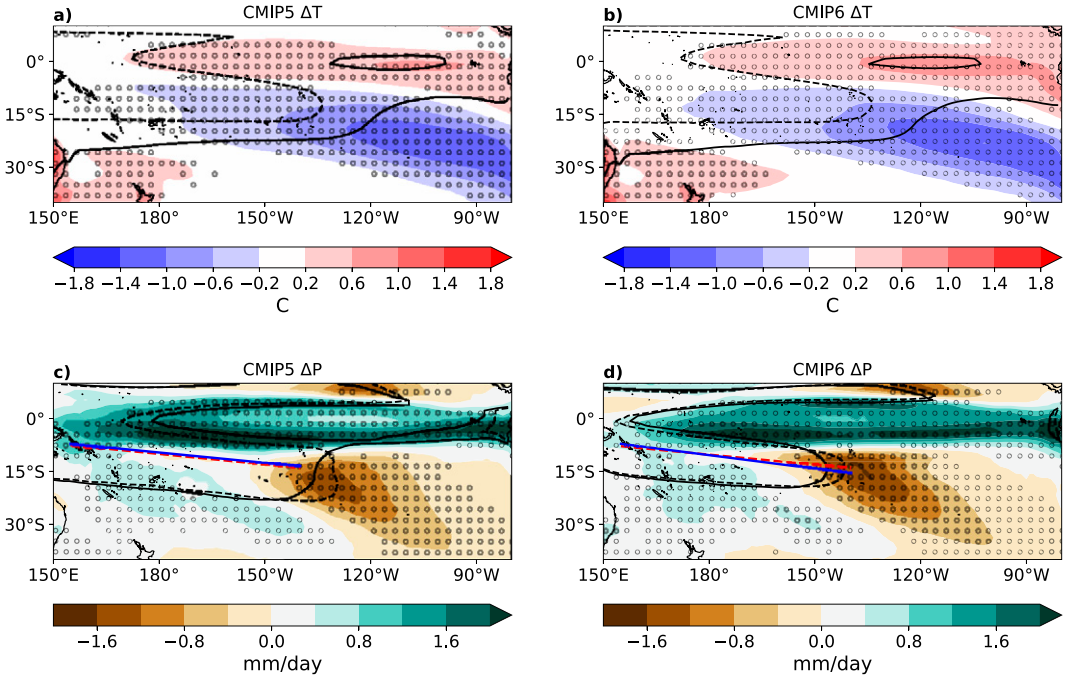

FIG. 3. Projected changes in (a),(b) relative surface temperature (°C) and (c),(d) absolute precipitation (mm day^{-1}), for the (left) CMIP5 MMM and (right) CMIP6 MMM. Stippling indicates where greater than two-thirds of models agree on the direction of change. Relative surface temperature change is calculated by subtracting the tropical mean SST change (30°S and 30°N). The contours represent the 28°C SST contour in (a) and (b) and the 5 mm day^{-1} contour in (c) and (d) for the future period (solid) and historical period (dashed). The diagnosed SPCZ for the MMM are shown for the future period (solid blue) and the historical period (dashed red).

and beyond? We correlate precipitation changes at every location with the changes in SPCZ position (Fig. 4d) and SPCZ slope (Fig. 4e) across the set of included models. Precipitation changes over most of the SPCZ region are highly anticorrelated with changes in the SPCZ position. Notably, the region with the strongest positive correlation with SPCZ position changes is in the equatorial Pacific. We provide the scatterplot of SPCZ position change against precipitation change at two locations as an example, one in the central equatorial Pacific (Fig. 4b), and the other in the SPCZ region itself (Fig. 4c). In contrast, the changes in the SPCZ slope appear to be only weakly related to South Pacific precipitation changes. Instead, the changes in the SPCZ slope correlate with changes in precipitation in the eastern Pacific basin, with a wave-like pattern extending into the North Pacific.

The results presented here show that large changes to the SPCZ in a warmer climate are possible as predicted by individual models, and that due to the strong disagreement between models, the ensemble mean change in the SPCZ may be deceptive when considering future risk. Although the changes in SPCZ slope and position are correlated, it is the change in SPCZ position that correlates best with changes to rainfall in the region. Next we will use the changes in SPCZ position to construct storylines of future changes to the SPCZ.

b. *Competing storylines of projected SPCZ change*

The multimodel mean change in the SPCZ (Fig. 3) is clearly the midpoint between very different potential outcomes (Fig. 4a). On one end of the spectrum an equatorward shift in the SPCZ with global warming whereby South Pacific Islands on the southern edge of the SPCZ could experience severe drying (e.g., up to 2.5 mm day^{-1} decrease at some locations, see Fig. 9). On the other end of the spectrum a poleward shift in the SPCZ with global warming whereby South Pacific Islands on the southern edge of the SPCZ could experience an increase in precipitation (e.g., up to 2.5 mm day^{-1} increase at some locations, see Fig. 9) and all its associated impacts. Therefore, describing the future of the SPCZ lends itself to a "storyline" approach to explore the future projection uncertainty space (Shepherd et al. 2018).

For the analysis presented next, we first combine all CMIP5 and CMIP6 models that were deemed suitable for diagnosing SPCZ changes using our methodology, as described in section 3. The remaining models are then divided into three groups, each portraying a different storyline of future SPCZ changes: one in which models exhibit a projected northward shift in the SPCZ (change in SPCZ position more than 0.5° northward), another in which models exhibit a projected southward shift in the SPCZ (change in SPCZ position more than 0.5° southward), and a third group where the SPCZ does not change position dramatically (SPCZ position changes less than 0.5° north- or southward). This results in similar sample sizes in each category (18 "northward," 15 "small shift," and 18 "southward" models; see Table A2 for classification).

In Fig. 5 we compare the MMM spatial patterns of change for the three storylines described above. Some key differences

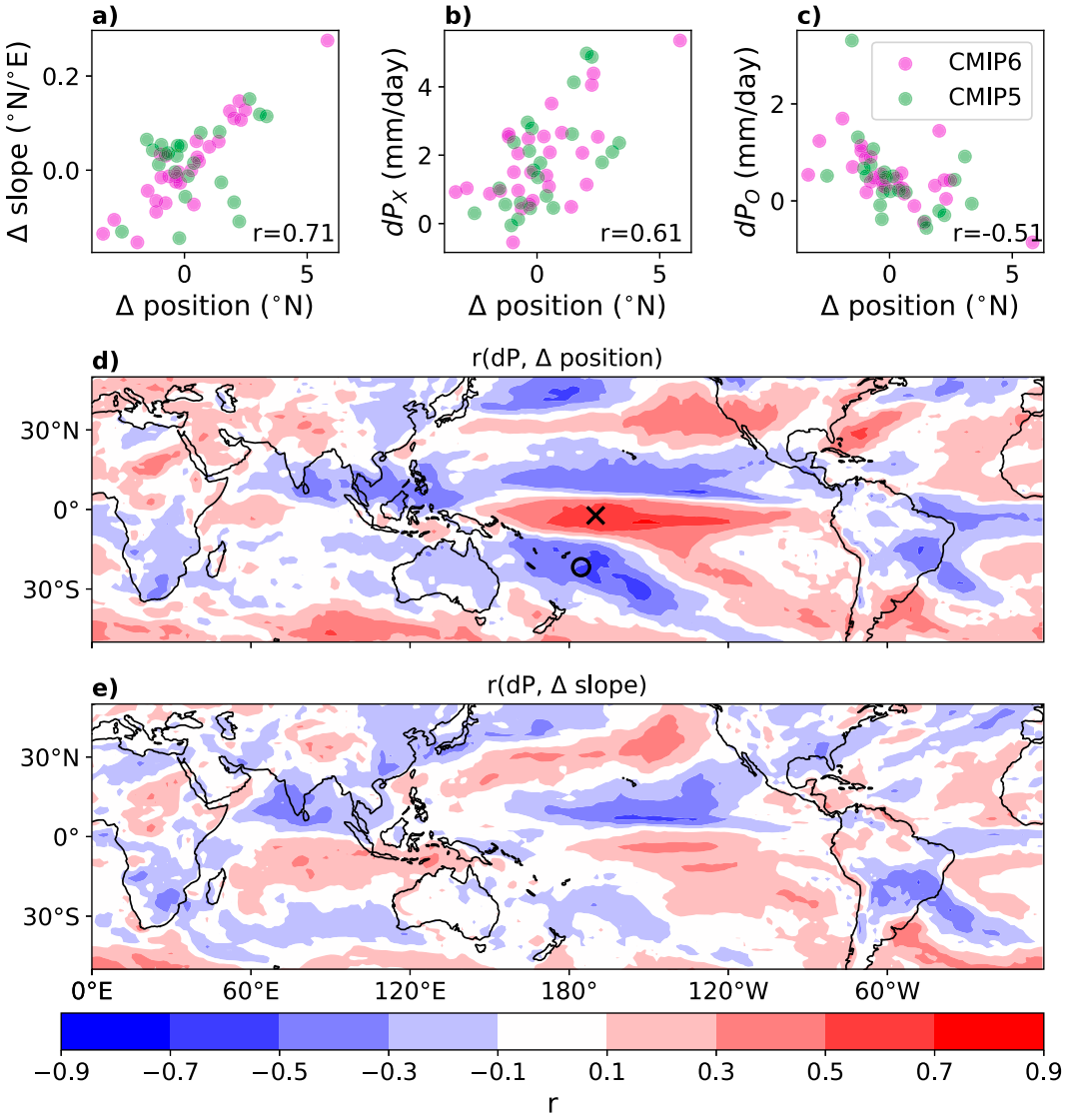

FIG. 4. The change in diagnosed SPCZ position (°N) vs (a) the change in diagnosed SPCZ orientation (°N/°E), (b) the change in absolute precipitation (mm day^{-1}) at position X (2.25°S,190°E), and (c) the change in precipitation at position O (21.75°S,184.5°E); these positions are marked in (d). The correlation between absolute precipitation change and (d) change in SPCZ position and (e) change in SPCZ slope, is shown for each location. The correlation r shown in (a)–(c) is for all models.

appear in the composites for these three groups of models. The northward models have a strong equatorial precipitation increase in the composite mean, but weak MMM precipitation changes in the SPCZ region, and poor model agreement on the changes in the southwest Pacific (Fig. 5a). The southward group has a weaker equatorial precipitation increase than the other two groups, and a clear increase in precipitation on the southern flank of the SPCZ, with strong model agreement on the pattern of change (Fig. 5c). This group of models has a stronger drying on the eastern edge of the SPCZ; however, all three groups consistently show a similar pattern of drying to the southeast of the SPCZ. The small shift MMM exhibits a small increase in precipitation over most of the SPCZ region (Fig. 5b). The three storylines thus represent a continuum of patterns of precipitation change.

The equatorial SST warming relative to the tropical mean (Figs. 5d–f) is largest in the northward MMM, and extends farthest into the west Pacific, while the southward MMM exhibits weaker relative SST warming at the equator. Historical SST biases are less clearly related to the chosen storylines; however, the southward group has larger tropical equatorial cool biases, while the northward group has a larger east Pacific warm bias on average (Figs. 5g–i). Associated with those historical SST biases, the southward group has the

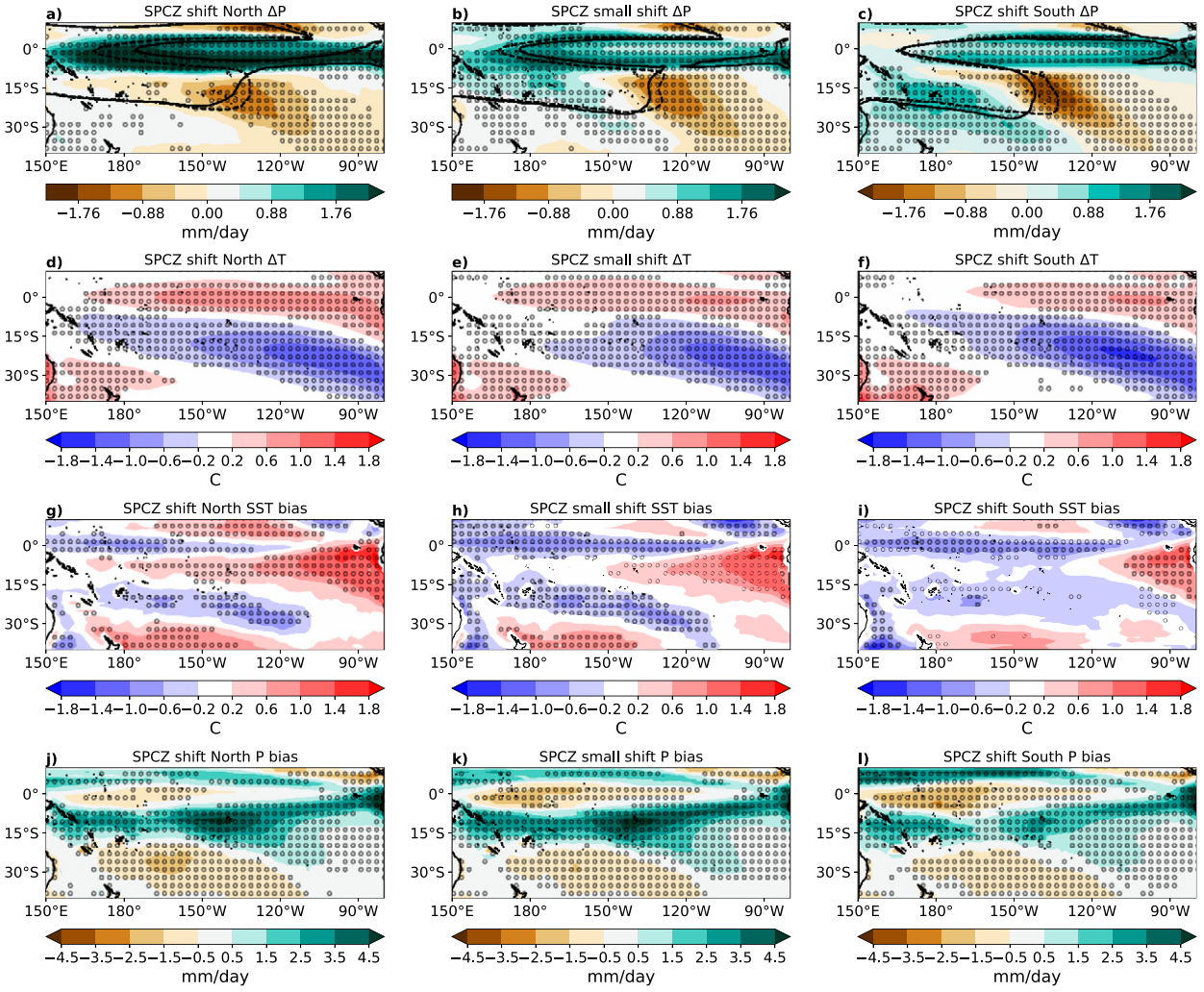

FIG. 5. Multimodel mean changes in (a)–(c) precipitation, (d)–(f) relative SST, (g)–(i) historical surface temperature biases, and (j)–(l) historical precipitation biases by model groups.The groups shown are (left) the northward-shifting SPCZ group, (center) the small shift SPCZ group, and (right) the southward-shifting SPCZ group. Stippling indicates where greater than two-thirds of models agree on the direction of change or bias. Relative SST changes are calculated by subtracting the mean change in SST between 30°S and 30°N in each model. The contours in (a)–(c) represent the 5 mm day^{-1} contours for the future period (solid) and historical period (dashed).

largest dry biases in the western tropical Pacific, while the northward group has the largest wet biases in the equatorial eastern Pacific (Figs. 5j–l).

c. *Links between SPCZ changes and ENSO*

How do the storylines of future SPCZ change relate to characteristics of interannual variability in the same set of models? In Fig. 6 we show the relationship between SPCZ position and the relative Niño-3.4 variability within each "storyline" model group. The northward group clearly has a visible trend in SPCZ position, indicated in Fig. 7a by a concentration of red dots on the upper-right side of the scatterplot, indicating more frequent northward-shifted SPCZ during strong El Niño events in the late twenty-first century, in agreement with the study of Cai et al. (2012) finding more "zonal SPCZ" events in future. The opposite is seen in the southward group, with more frequent southward-shifted SPCZ during strong La Niña events in the late twenty-first century. The small shift group shows no obvious trend in either SPCZ position or relative Niño-3.4 index. The divergent changes in frequency of extreme northward and southward SPCZ displacement on interannual time scales between the northward- and southward-shifted mean SPCZ states could result in quite different regional climate impacts between these two storylines of future SPCZ change.

In Fig. 7 we correlate SPCZ position changes with regional and global surface temperature characteristics in each model. Although mean state biases in the western Pacific are thought to be important for regional precipitation changes (e.g., Chadwick et al. 2014), the SPCZ position changes are not strongly correlated with the historical cold-tongue index (Fig. 7a). Similarly, no relationship is found between the change in SPCZ position

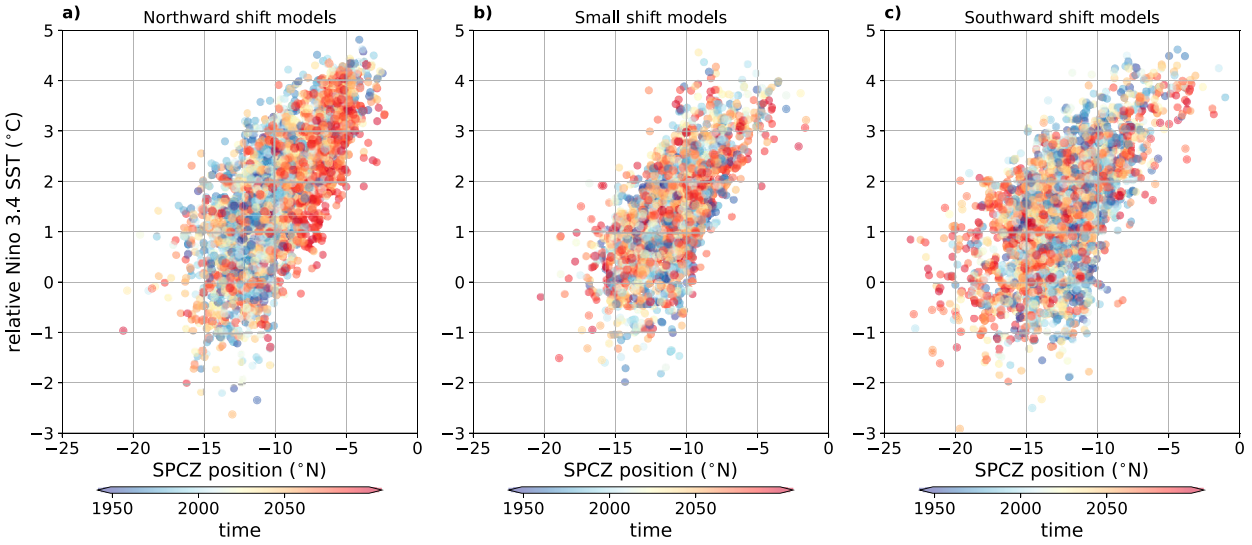

FIG. 6. Diagnosed SPCZ position vs relative Niño-3.4 SST for each year in the (a) northward, (b) small shift, and (c) southward groups of models. Shading indicates the year between 1950 and 2099.

and change in the zonal gradient in SST across the equatorial Pacific (Fig. 7b). However, confirming the results from Fig. 6, the change in Niño-3.4 region SST relative to the tropical mean is correlated ($r = 0.43$) with the change in mean SPCZ position across models (Fig. 7c). This suggests that enhanced central equatorial Pacific warming may favor an equatorward shift in the SPCZ. We also investigate the relationship between equilibrium climate sensitivity (ECS, values given in Table A2 and taken from Meehl et al. 2020) and SPCZ position in the models (Fig. 7d), finding no relationship between ECS and the change in SPCZ position ($r = 0.06$).

d. Moisture budget decomposition

Next we investigate the role of dynamic versus thermodynamic processes in SPCZ precipitation change for each of the three storyline model groups defined in section 4b. The decomposition of precipitation changes using a moisture budget approach is calculated for individual models, and then averaged. In Fig. 8 we present the multimodel mean of the change in moisture budget terms, according to three model groups. Due to data availability we analyze a reduced set of models for each group (13/18 northward, 12/15 small shift, and 15/18 southward models, see Table A2). The thermodynamic term (∂TH) tends to contribute to increases in precipitation in the SPCZ, enhancing locations of climatological heavy precipitation. The mean circulation dynamics term (∂MCD) both enhances and reduces precipitation in different parts of the SPCZ in each group. The changes in the other terms are small on average compared to ∂TH and ∂MCD.

The northward group simulates larger equatorial Pacific precipitation increases on average, as well as a slightly larger increase in the thermodynamic term (∂TH). However, the most striking difference between the groups is the change in the mean circulation dynamics term (∂MCD). The patterns show not just changes in the SPCZ region itself but coherent patterns over the ITCZ, equator and farther afield.

To further emphasize the reliance of local precipitation projections on the change in mean circulation dynamics, in Fig. 9 we present the change in moisture budget terms over localized regions (marked in Fig. 8) near Vanuatu (western SPCZ), Tuvalu (northern SPCZ), the Cook Islands (central SPCZ), and the Pitcairn Islands (eastern SPCZ). For Vanuatu, Tuvalu, and the Cook Islands we observe that the change in precipitation to first order is determined by ∂TH and ∂MCD, since the other terms are smaller. All three countries are located on the western portion of the model-mean SPCZ, where the change in the thermodynamic component is positive and of similar magnitude on average in each group. The mean circulation dynamics component of precipitation change has a much wider spread, and controls the variation in precipitation change between groups. Similarly for the Pitcairn Islands, the change in precipitation is determined by ∂MCD, although ∂TH is small, and the eddy covariant term (∂COV) is the second largest component. The key result shown in this analysis is that the large uncertainty in the change in mean circulation dynamics is the major factor in the large uncertainty for changes in mean precipitation in the SPCZ region.

The indices explored in Fig. 7 appear to relate only weakly to changes in SPCZ position, yet they are believed to be important factors affecting precipitation in the South Pacific. In Fig. 10 we explore the relationship between these indices and the components of precipitation change using the moisture budget decomposition terms. ECS is found to correlate to changes in precipitation in parts of the SPCZ, and this is shown to be primarily due to changes in the thermodynamic term (∂TH), although partly offset by changes in the mean circulation and eddy covariance terms (∂MCD and ∂COV). So although ECS is not strongly related to SPCZ position (Fig. 7), it does in fact relate to changes in the intensity of the SPCZ. The change in Niño-3.4 region SST relative to the tropical

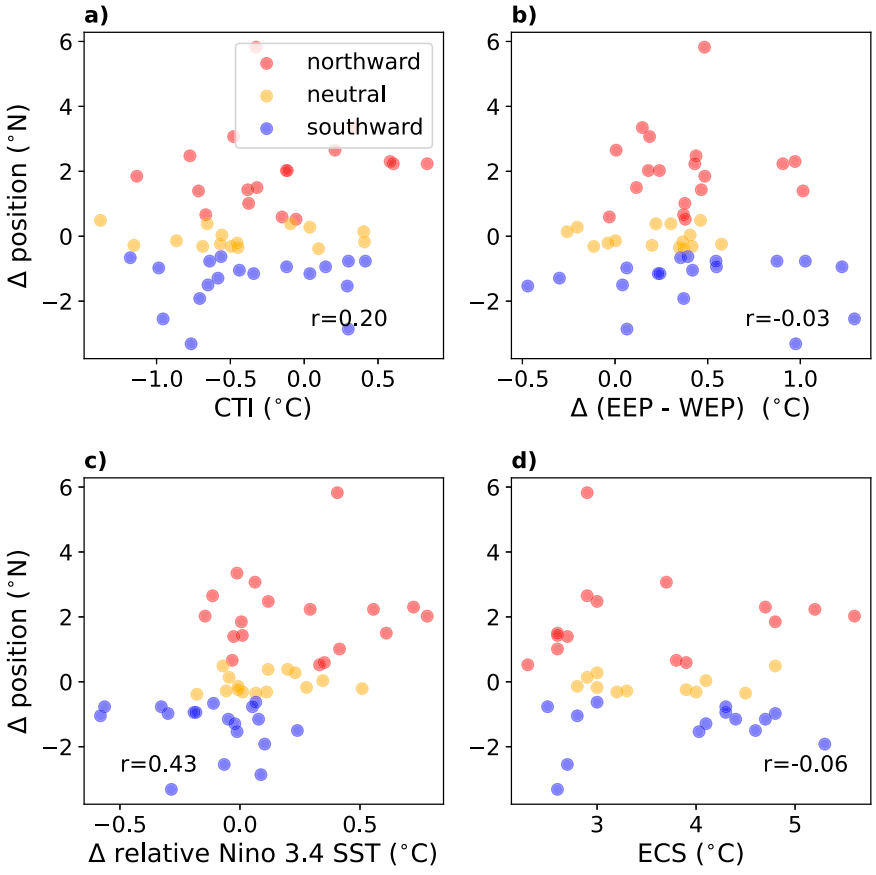

FIG. 7. Projected change in SPCZ position plotted against (a) historical climatology cold tongue index (CTI), (b) change in zonal gradient in the equatorial Pacific, (c) change in Niño-3.4 region SST relative to the tropical mean change, and (d) equilibrium climate sensitivity (ECS) in each model. All indices are defined in section 2.

mean change (Δ rel. N3.4) relates strongly to SPCZ position changes (Fig. 7), and through the moisture budget decomposition we find that this relationship is largely related to changes in the mean circulation dynamics (∂MCD) term. We find that the historical climatological cold tongue index (CTI) relates poorly to precipitation changes, and to all terms in the moisture budget decomposition. The change in zonal gradient in the equatorial Pacific [∂(EEP − WEP)] correlates to changes in SPCZ precipitation, but this relationship appears to be related to several terms (the evaporation, thermodynamic, and mean circulation dynamic terms).

The storylines presented here and the subsequent analyses of their characteristics suggest that future changes to the SPCZ depend heavily on dynamical changes in the South Pacific atmosphere. In Fig. 11 we investigate some aspects of these dynamical changes by storylines. While all three groups exhibit similar patterns of change, some differences emerge in the multimodel means for each storyline. The change in velocity potential at 250 hPa provides an indication of changes in the divergent circulation, with negative velocity potential indicating an upward anomaly in air motion. All storylines exhibit an increase in 250-hPa velocity potential over the western equatorial Pacific, and a decrease over the eastern equatorial Pacific, suggesting a weakening of the Walker circulation. However, the strength of the equatorial east–west gradient of the change in 250-hPa velocity potential is largest for the northward group of models. The change in 500-hPa streamfunction, indicating the change in horizontal circulation in the midtroposphere, also shows a similar pattern between storylines. However, one key difference is the anticyclonic change in streamfunction in the Southern Pacific, as well as the increase in cyclonic streamfunction farther poleward. This pattern is weakest for the northward group, and strongest for the southward group of models. The southward group also has the strongest anticylonic change in streamfunction in the Southern Hemisphere eastern equatorial Pacific. The change in winds at 850 hPa mirror the 500-hPa streamfunction changes, with the southward group displaying the largest changes in the midlatitudes, perhaps indicative of a stronger poleward shift or strengthening of the jet stream.

5. Summary, discussion, and conclusions

We evaluated the South Pacific convergence zone (SPCZ) in CMIP5 and CMIP6 models, and investigated future projections of the SPCZ under high emission scenarios (RCP8.5 and

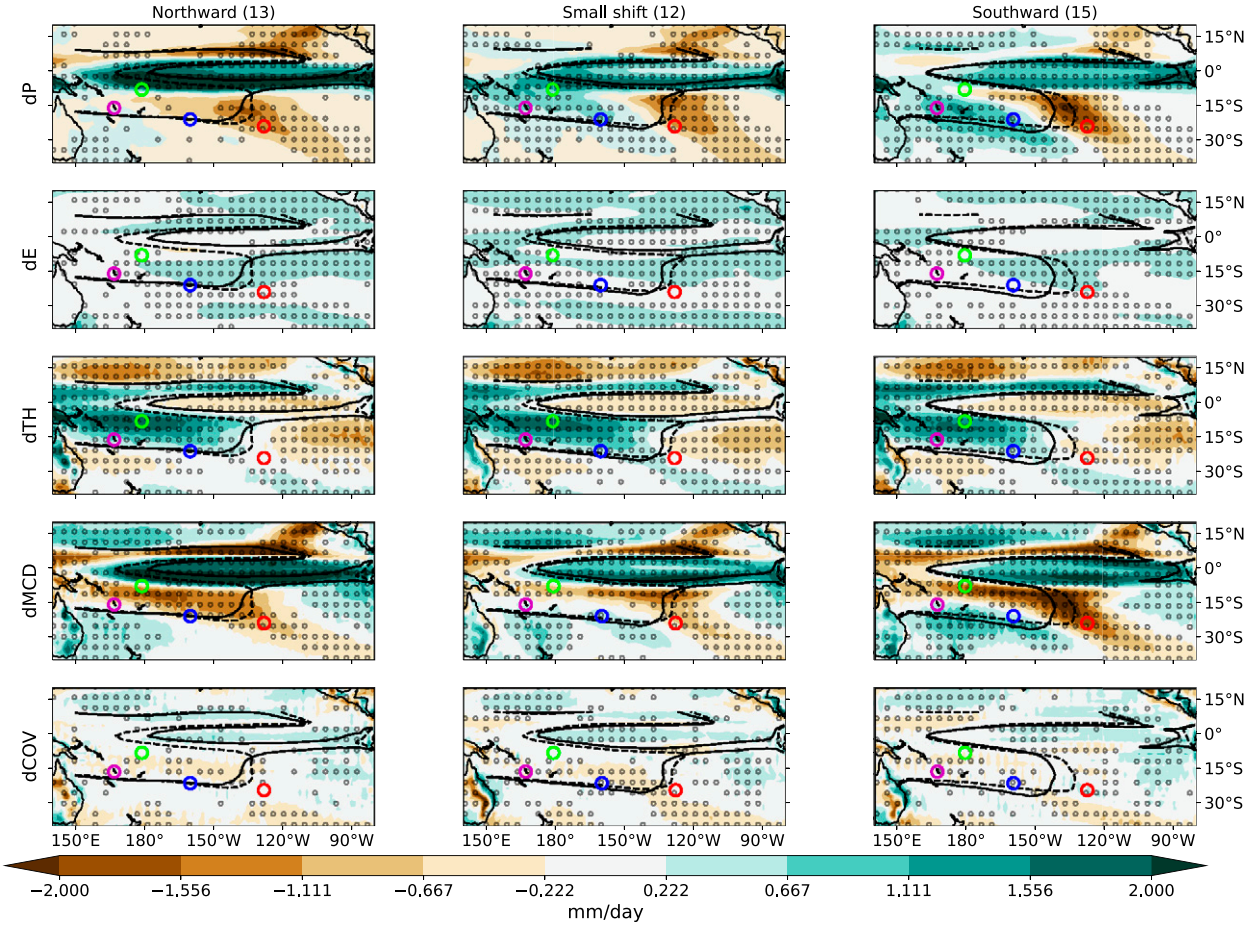

FIG. 8. Multimodel mean (MMM) precipitation changes (∂P) for the (left) northward, (center) small shift, and (right) southward groups of models, as well as change in moisture budget decomposition terms for evaporation (∂E), thermodynamic component (∂TH), mean circulation dynamic component (∂MCD), and covarying term (∂COV). Stippling indicates where greater than two-thirds of models agree on the direction of change. The black contours represent the 5 mm day^{-1} contours for the future period (solid) and historical period (dashed). Purple, green, blue, and red circles indicate case study locations, respectively: Vanuatu (16°S, 167°E), Tuvalu (8°S, 179°E), Cook Islands (21°S, 160°W), and Pitcairn Islands (24°S, 128°W).

SSP5–8.5). We then determined the extent to which the simulated changes were related to regional and global features of interest such as tropical SST patterns and equilibrium climate sensitivity. Models were categorized according to their future changes and investigated using a storyline approach. These storylines represent a simplified categorization of plausible diverging future changes to the SPCZ with global warming. The purpose of the storylines presented here is twofold. First, we present storylines that could be useful for next-users of SPCZ climate change projections that could benefit from a narrative-based rather than probabilistic approach. Second, we investigate the reasons behind these diverging storylines, to provide some insights that may eventually help with reducing the uncertainty for the very challenging problem of projecting SPCZ changes with global warming.

Some aspects of the precipitation and surface temperature biases are found to be improved in the available CMIP6 ensemble compared with the CMIP5 ensembles (Figs. 1 and 2). In particular, the pattern correlation coefficient of precipitation in models compared to GPCP observations in the SPCZ region is improved in CMIP6 models. However, longstanding biases in the equatorial southeastern Pacific remain, in particular, excessive precipitation in the eastern Pacific during the austral summer—a well-documented bias in climate models, which is related to the double-ITCZ bias (e.g., Li and Xie 2014; Samanta et al. 2019; Fiedler et al. 2020). Similarly the December–February "cold tongue bias" in the equatorial western Pacific is not improved between the two ensembles in the multimodel mean, and is in fact degraded east of the date line. This contrasts with the improvement between the two ensembles found by Grose et al. (2020) using the same cold tongue index as the present study, but applied to the June–November season.

The position and slope of the SPCZ were estimated in observations and models at both climatological and interannual time scales following a simple and well-established line-fitting method (Brown et al. 2011; Vincent et al. 2011). Overall, we found most of the models surveyed to be suitable for our diagnostic analyses

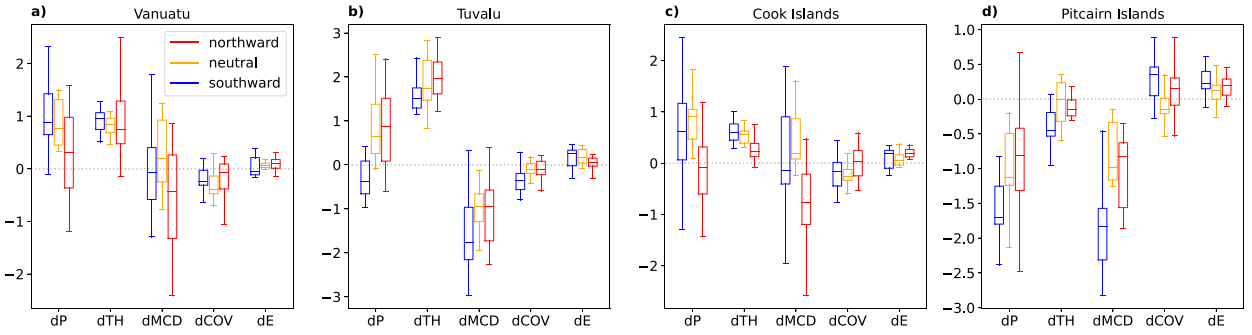

FIG. 9. Change in moisture budget terms for each group of models, for an example region around Vanuatu (16°S, 167°E), Tuvalu (8°S, 179°E), Cook Islands (21°S, 160°W), and Pitcairn Islands (24°S, 128°W). Boxes display the interquartile range and the median, while the whiskers show the minimum of either 1.5 times the interquartile range or the farthest data point.

of SPCZ changes in a warmer climate. We find no clear improvement in the diagnosed SPCZ slope and position in CMIP6 models compared to CMIP5 models, with all models simulating an SPCZ slope that is more zonal than observed; however, most outliers (very poor models) were from the CMIP5 ensemble (Fig. 2). Overly zonal SPCZ orientation, along with the double ITCZ bias, is a longstanding problem in climate models and has been related to zonal and meridional SST gradients in the Pacific (Cai et al. 2012), and even convection parameterization (Möbis and Stevens 2012).

However, does an improved historical simulation of the SPCZ help to constrain future projections for the region?

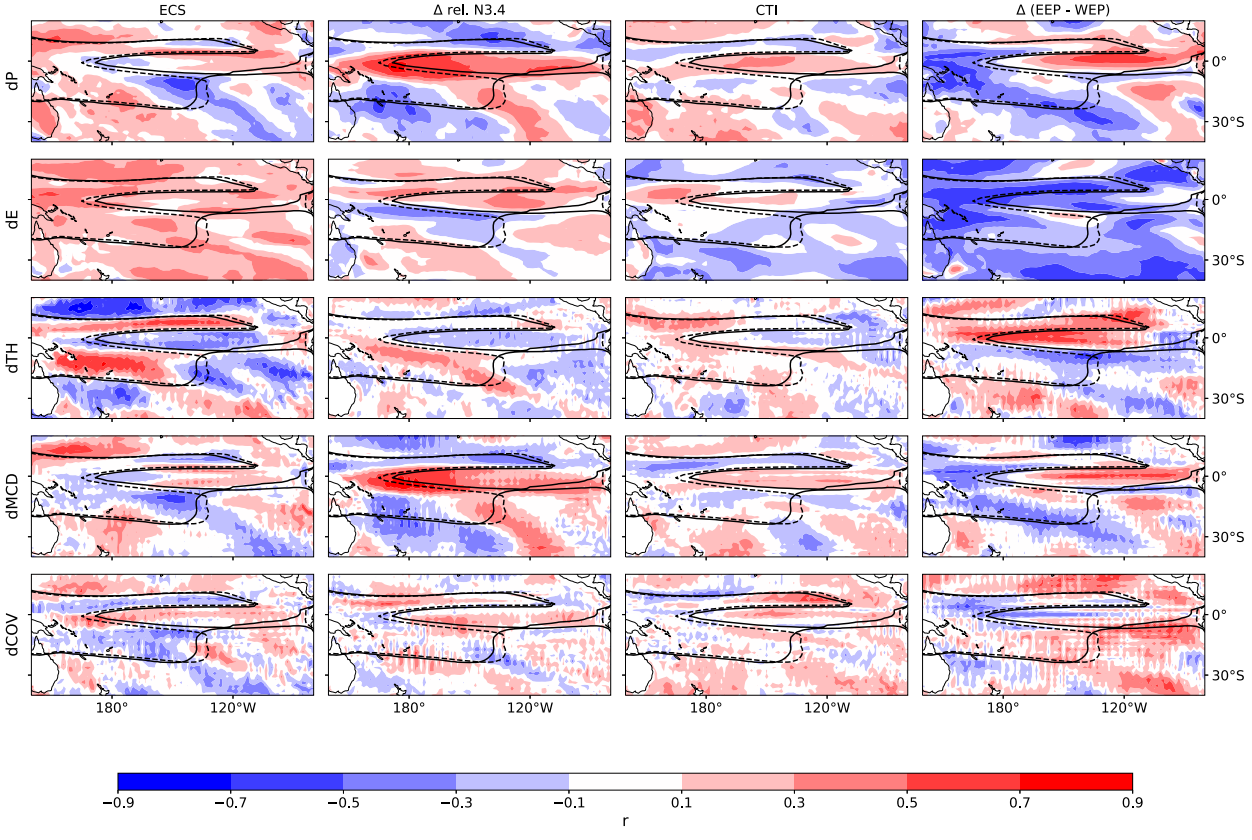

FIG. 10. The inter-model correlation (r) between the change in moisture budget decomposition terms (in rows) against selected indices (in columns). Shown from top to bottom are changes in precipitation (∂P), evaporation (∂E), thermodynamic component (∂TH), mean circulation dynamic component (∂MCD), and the covarying term (∂COV). Shown from left to right are equilibrium climate sensitivity (ECS), change in Niño-3.4 region SST relative to the tropical mean change (Δ rel. N3.4), historical climatology cold tongue index (CTI), and change in zonal gradient in the equatorial Pacific [Δ(EEP − WEP)]. The black contours represent the multimodel mean 5 mm day^{-1} contours for the future period (solid) and historical period (dashed).

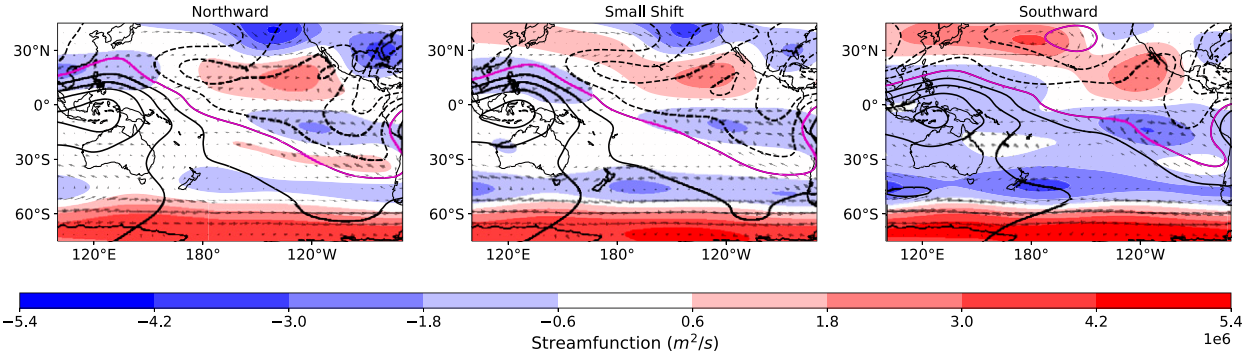

FIG. 11. Multimodel mean (MMM) changes in 500-hPa streamfunction (colors), 250-hPa velocity potential (black contours), and 850-hPa winds (gray vectors) for the composites of the three groups of models. All quantities are presented as the difference between the future period (2050–99) and historical period (1950–99). The magenta contour represents the zero change in 250-hPa velocity potential, while the black contours have an interval of 5×10^5 m^2 s^{-1} (dashed lines representing negative change).

Although there are incremental improvements in the mean climate of the South Pacific in the CMIP6 ensemble compared to the CMIP5 ensemble, we did not find a noticeable difference in the ensemble-mean projected changes of the diagnosed SPCZ (Fig. 3). The MMM changes are small in both ensembles, belying much larger, albeit compensating, positive and negative changes to the SPCZ in individual models (Fig. 4a). Inter-model disagreement on SPCZ changes has also been noted in previous generations of climate models (Brown et al. 2012, 2013; Widlansky et al. 2013).

We further explore the diverging projected changes to the SPCZ using a "storyline" approach (Shepherd et al. 2018). Using changes in the position of the SPCZ with global warming to distinguish possible futures, we group the combined CMIP5 and CMIP6 models into three storylines: a northward-shifting SPCZ, a southward-shifting SPCZ, and a small shift in the SPCZ. We chose to use the SPCZ position to construct these storylines for two reasons; first, the change in position was highly correlated to precipitation change over the SPCZ, while the change in slope was not (Figs. 5d,e). Second, precipitation changes in the region are nonuniform, with both positive and negative changes found on either side of the SPCZ. Such nonuniformity made it problematic to use a simple area average in precipitation as a means of grouping models into coherent storylines. For brevity we will now focus our discussion on the two extremes of SPCZ changes: the southward and northward groups of models.

The northward group exhibited weaker changes in the SPCZ region but a much stronger change in precipitation in the equatorial Pacific. The southward group tended to exhibit a wetter SPCZ, and a comparatively weaker increase in precipitation in the equatorial Pacific (Fig. 5). We also note that the northward models simulate an increased frequency of extreme northward displaced SPCZ during future strong El Niño events, while the southward models simulate an increased frequency of extreme southward displaced SPCZ during future strong La Niña events (Fig. 6).

Comparison of mean state and SPCZ changes indicates that the models in which the SPCZ moves northward have an enhanced equatorial Pacific warming (estimated using Niño-3.4 SST relative to the tropical mean), rather than an increased zonal gradient over the equatorial Pacific (Fig. 7). Understanding the enhanced equatorial warming (EEW) response in climate models, which is largest in the Pacific, is thought to be key to reducing uncertainty in regional tropical and subtropical projections (e.g., Grose et al. 2014; Zhou et al. 2019). However, it is currently poorly constrained by theory, observations, and models, especially at regional scales. Given the projection depends on this poorly understood feature of the tropical SST response, we cannot currently use equatorial warming patterns as a constraint on whether the northward or southward SPCZ shift is more plausible.

We also found that changes in the SPCZ position were not correlated with equilibrium climate sensitivity (ECS) estimates for each model (Fig. 7). Although ECS was found to correlate strongly with the thermodynamic component of precipitation change, this effect appeared to be partially offset by dynamical changes, leading to a weak and regionally varied relationship with precipitation change (Fig. 10). To first order one might have expected the SPCZ precipitation to increase in proportion to global warming due to the "wet-gets-wetter" mechanism, whereby a warmer atmosphere can lead to enhanced precipitation through increases in water vapor due to the Clausius–Clapeyron relation (Chou and Neelin 2004; Held and Soden 2006). However, this thermodynamic response only tends to hold at the largest scales, with regional changes typically being driven by dynamical feedbacks in models such as the "upped-ante" mechanism (Chou et al. 2009). Complicating matters further is the possible relationship between ECS and regional SST patterns (Dong et al. 2020).

Widlansky et al. (2013) framed the projected changes to the SPCZ in terms of competing mechanisms: suggesting that dynamic changes will dominate at lower warming levels leading to decreases in SPCZ precipitation, while the thermodynamic changes will dominate at higher warming levels to produce a net increase in average precipitation in the SPCZ region. Here we have analyzed the highest emission scenarios for the late twenty-first century, and therefore we are considering the

TABLE A1. The details of models and evaluation of SPCZ simulation in historical climate. Model name, MIP (CMIP5 or CMIP6), precipitation correlation between model and observations over SPCZ region (30°S–0°, 155°E–140°W), surface temperature correlation between model and observations over SPCZ region, precipitation root-mean-square error between model and observations over SPCZ region, surface temperature root-mean-square error between model and observations over SPCZ region, SPCZ slope (°N/°E), and SPCZ position (°N) calculated over SPCZ region following method outlined in section 2.

Model	MIP	*P* corr	*T* corr	*P* RMSE	*T* RMSE	Slope (°N/°E)	Position (°N)
ACCESS-CM2	CMIP6	0.82	0.98	2.91	0.39	−0.06	−8.98
ACCESS-ESM1–5	CMIP6	0.85	0.98	3.05	0.46	−0.10	−11.81
ACCESS1–0	CMIP5	0.89	0.98	2.58	0.94	−0.14	−10.34
ACCESS1–3	CMIP5	0.88	0.98	2.83	0.71	−0.03	−10.59
AWI-CM-1–1-MR	CMIP6	0.79	0.96	2.88	0.79	−0.14	−13.34
BCC-CSM1–1	CMIP5	0.86	0.96	2.90	0.58	−0.14	−10.52
BCC-CSM1–1-M	CMIP5	0.71	0.97	2.92	0.76	−0.04	−9.33
BCC-CSM2-MR	CMIP6	0.81	0.96	3.51	0.76	−0.06	−9.37
BNU-ESM	CMIP5	0.63	0.93	2.43	0.74	−0.08	−8.98
CAMS-CSM1–0	CMIP6	0.74	0.98	2.97	0.54	−0.07	−9.30
CanESM2	CMIP5	0.79	0.97	2.46	0.87	−0.14	−10.10
CanESM5	CMIP6	0.79	0.98	2.59	0.63	−0.07	−10.80
CCSM4	CMIP5	0.81	0.99	1.61	0.37	−0.12	−9.82
CESM1-BGC	CMIP5	0.82	0.99	1.59	0.48	−0.10	−10.24
CESM1-CAM5	CMIP5	0.73	0.98	1.90	0.58	−0.02	−10.90
CESM2	CMIP6	0.91	0.98	1.34	0.64	−0.15	−10.97
CESM2-WACCM	CMIP6	0.87	0.98	1.67	0.54	−0.09	−10.94
CMCC-CESM	CMIP5	0.77	0.97	2.47	0.83	−0.04	−12.12
CMCC-CM	CMIP5	0.86	0.96	2.69	0.73	−0.20	−9.75
CMCC-CM2-SR5	CMIP6	0.77	0.96	1.81	0.82	−0.03	−11.42
CMCC-CMS	CMIP5	0.88	0.99	1.92	0.26	−0.13	−11.84
CNRM-CM5	CMIP5	0.88	0.99	1.16	0.64	−0.10	−9.44
CNRM-CM6–1	CMIP6	0.88	0.97	1.48	0.95	−0.13	−9.99
CNRM-ESM2–1	CMIP6	0.84	0.96	1.67	0.70	−0.12	−9.96
CSIRO-Mk3–6-0	CMIP5	0.60	0.89	4.57	1.91	−0.08	−12.82
EC-Earth3	CMIP6	0.93	0.99	1.11	0.60	−0.11	−12.19
EC-Earth3-Veg	CMIP6	0.89	0.98	1.33	0.64	−0.13	−12.30
FGOALS-f3-L	CMIP6	0.81	0.96	1.92	1.55	−0.14	−9.44
FGOALS-g3	CMIP6	0.88	0.98	1.87	0.85	−0.23	−12.12
FIO-ESM-2–0	CMIP6	0.75	0.99	1.93	0.52	−0.03	−11.15
GFDL-CM3	CMIP5	0.74	0.99	1.96	0.51	−0.05	−11.74
GFDL-CM4	CMIP6	0.89	0.99	1.52	0.92	−0.13	−12.65
GFDL-ESM2G	CMIP5	0.55	0.95	3.18	0.92	−0.10	−15.47
GFDL-ESM2M	CMIP5	0.77	0.99	1.83	0.53	0.01	−12.23
GFDL-ESM4	CMIP6	0.87	0.99	1.48	0.50	−0.12	−12.23
GISS-E2-H	CMIP5	0.54	0.96	2.45	0.55	0.01	−11.04
GISS-E2-H-CC	CMIP5	0.52	0.96	2.58	0.55	0.01	−10.80
GISS-E2-R	CMIP5	0.58	0.96	2.55	0.60	−0.13	−10.13
GISS-E2-R-CC	CMIP5	0.58	0.96	2.57	0.66	−0.16	−9.51
HadGEM2-AO	CMIP5	0.89	0.98	3.00	0.38	−0.13	−11.95
HadGEM2-CC	CMIP5	0.91	0.98	2.81	0.91	−0.15	−10.97
INM-CM4–8	CMIP6	0.52	0.81	2.90	1.53	0.05	−11.28
INM-CM5–0	CMIP6	0.58	0.89	2.67	1.46	0.06	−10.73
INMCM4	CMIP5	0.81	0.98	2.20	0.49	0.03	−9.61
IPSL-CM5A-LR	CMIP5	0.82	0.97	2.00	0.88	−0.13	−11.81
IPSL-CM5A-MR	CMIP5	0.86	0.98	1.70	0.65	−0.18	−12.89
IPSL-CM5B-LR	CMIP5	0.87	0.97	2.00	0.63	−0.14	−9.99
IPSL-CM6A-LR	CMIP6	0.81	0.97	1.90	0.87	−0.07	−10.24
KACE-1–0-G	CMIP6	0.82	0.98	2.55	0.53	−0.08	−9.19
MIROC-ES2L	CMIP6	0.73	0.95	1.68	0.82	−0.04	−8.77
MIROC-ESM	CMIP5	0.34	0.73	3.27	1.95	0.12	−13.34
MIROC-ESM-CHEM	CMIP5	0.36	0.71	3.29	1.99	−0.08	−16.59
MIROC5	CMIP5	0.78	0.98	1.61	1.07	−0.19	−14.11
MIROC6	CMIP6	0.80	0.99	1.69	0.86	−0.07	−13.24
MPI-ESM-LR	CMIP5	0.58	0.92	3.27	1.06	−0.09	−14.25

TABLE A1. (*Continued*)

Model	MIP	*P* corr	*T* corr	*P* RMSE	*T* RMSE	Slope (°N/°E)	Position (°N)
MPI-ESM-MR	CMIP5	0.57	0.94	3.16	0.81	−0.07	−14.39
MPI-ESM1–2-HR	CMIP6	0.85	0.99	2.44	0.42	−0.08	−12.26
MPI-ESM1–2-LR	CMIP6	0.82	0.99	2.65	0.90	−0.10	−12.12
MRI-CGCM3	CMIP5	0.72	0.97	3.22	0.47	−0.04	−10.24
MRI-ESM1	CMIP5	0.73	0.97	3.15	0.53	−0.04	−10.20
NESM3	CMIP6	0.77	0.90	2.38	1.07	−0.06	−12.92
NorESM1-M	CMIP5	0.90	0.99	1.13	0.86	−0.21	−13.03
NorESM1-ME	CMIP5	0.86	0.99	1.40	1.19	−0.23	−13.48
NorESM2-MM	CMIP6	0.86	0.99	1.86	0.43	−0.12	−11.67
TaiESM1	CMIP6	0.79	0.99	1.58	0.39	−0.09	−10.90
UKESM1–0-LL	CMIP6	0.86	0.99	2.08	0.67	−0.05	−10.90

changes at high global warming levels. We found that dynamic changes continue to be of primary importance in a severely warmer world. A decomposition of projected precipitation changes into moisture budget terms helps quantify where the uncertainties in SPCZ projections originate (Fig. 8). While there is strong agreement on model SPCZ precipitation increases due to thermodynamic changes, the changes in the mean circulation dynamics are the primary source of uncertainty for projected changes in precipitation in the SPCZ region, especially at the scale of Pacific Island states (e.g., Fig. 9). The dynamic term also dominates ensemble mean changes in CMIP5 and CMIP6 precipitation (Fig. S7). Understanding the regional circulation response to global warming, as well as pattern changes to SSTs, has been identified as the key to reducing regional projection uncertainty in several studies (e.g., Seager et al. 2010; Chadwick et al. 2014; Grose et al. 2014; Chung and Power 2016).

Further analysis of the differences between the SPCZ storylines indicated that changes to atmospheric circulation in both the tropics and extratropics may play a role. In the tropics it was shown that the change in the mean circulation dynamical contribution to precipitation in the South Pacific was strongly related to changes in relative Niño 3.4 SSTs (Fig. 10). An analysis of the dynamical changes in each storyline (Fig. 11) indicated that changes in the SPCZ may be related to differences in changes to the midlatitude jet stream. Interactions between the westerly winds and the downstream topography are thought to impact the southeast Pacific dry zone and therefore influence both the SST pattern and eastern SPCZ precipitation (Takahashi and Battisti 2007). Future studies could consider the interaction between the westerly winds and the Andes in climate models as a potential constraint on SPCZ projections.

To summarize, we constructed storylines centered around the late-twenty-first century changes to the SPCZ position, showing that the thermodynamic changes tend to be consistent between groups of models, while the mean circulation dynamical changes in the South Pacific vary quite substantially according to model group. We also note that for some locations (e.g., the far-eastern edge of the SPCZ) models consistently predict large reductions in precipitation, mostly associated with dynamical changes (stronger trade winds, see Brown et al. 2013 for discussion). To span the range of plausible future SPCZ projections, both storylines (northward and southward movement of the SPCZ) should be considered when examining future change for planning purposes.

Some caveats apply to the results presented in this study. The SPCZ identification scheme applied is unable to separate precipitation due to the model SPCZ from precipitation associated with regional biases such as the double ITCZ, present in some models, particularly when this secondary Southern Hemisphere ITCZ in the eastern Pacific extends to the central South Pacific and merges with the SPCZ. We attempt to minimize the influence of the double ITCZ bias by identifying models that have a simulated SPCZ that has an unrealistic slope or position or have a poor regional representation of precipitation patterns (Fig. 2) and excluding those models from subsequent analyses. We do not attempt here to estimate model independence (e.g., Bishop and Abramowitz 2013; Herger et al. 2018), and we note some correlated biases within our chosen groups of models (Fig. 5).

The storyline approach developed in this study represents only one approach to separate the ensemble into meaningful groupings. Our choice of grouping is based on the projection of interest (change in SPCZ position) rather than any specific physical processes. If multiple pathways to the same change in precipitation pattern occur within the ensemble, our method would not separate them. An alternative, process-based approach would be required to provide insight into the mechanisms producing different shifts in SPCZ position.

We propose here that to improve projections for the SPCZ region we must first gain greater clarity on the processes that lead to SST pattern changes such as enhanced equatorial warming in the Pacific, and the dynamical response of the atmosphere to those pattern changes. Future work could focus on evaluating the realism of the modeled dynamical response to changed Pacific SST patterns in a warmer future climate.

While uncertainty remains about the most plausible future projections for the SPCZ, an approach based on storylines of different possible SPCZ projections can provide a useful source of information about future risk to assist planning and adaptation efforts in the South Pacific.

Acknowledgments. We thank Christine Chung and Eun-Pa Lim for useful comments on the manuscript. We acknowledge the support of the Australian government's National

TABLE A2. Change in model SPCZ, model group. Model name, MIP (CMIP5 or CMIP6), change in SPCZ slope (°N/°E) between historical and future climate, change in SPCZ position (°N) between historical and future climate, model group (exclude, northward, southward, small shift), moisture budget calculated, and equilibrium climate sensitivity (ECS) values taken from Meehl et al. (2020).

Model	MIP	Slope change (°N/°E)	Position change (°N)	Group	Moisture budget	ECS
ACCESS-CM2	CMIP6	−0.06	−1.15	Southward		4.7
ACCESS-ESM1–5	CMIP6	0.02	0.59	Northward		3.9
ACCESS1–0	CMIP5	0.08	0.66	Northward		3.8
ACCESS1–3	CMIP5	−0.14	−0.21	Small shift		
AWI-CM-1–1-MR	CMIP6	−0.01	−0.31	Small shift	Yes	3.2
BCC-CSM1–1	CMIP5	0.05	−0.14	Small shift	Yes	2.8
BCC-CSM1–1-M	CMIP5	−0.01	0.14	Small shift	Yes	2.9
BCC-CSM2-MR	CMIP6	0.00	0.28	Small shift	Yes	3
BNU-ESM	CMIP5	0.10	1.95	Exclude		4.1
CAMS-CSM1–0	CMIP6	0.03	0.52	Northward	Yes	2.3
CanESM2	CMIP5	0.12	3.07	Northward	Yes	3.7
CanESM5	CMIP6	0.11	2.02	Northward	Yes	5.6
CCSM4	CMIP5	0.15	2.65	Northward	Yes	2.9
CESM1-BGC	CMIP5	0.11	3.35	Northward	Yes	
CESM1-CAM5	CMIP5	−0.06	0.03	Small shift	Yes	4.1
CESM2	CMIP6	0.15	2.23	Northward		5.2
CESM2-WACCM	CMIP6	0.11	2.30	Northward	Yes	4.7
CMCC-CESM	CMIP5	−0.11	2.23	Northward		
CMCC-CM	CMIP5	0.05	−0.94	Southward	Yes	
CMCC-CM2-SR5	CMIP6	−0.11	−2.86	Southward	Yes	
CMCC-CMS	CMIP5	0.00	−0.38	Small shift		
CNRM-CM5	CMIP5	0.05	−0.28	Small shift	Yes	3.3
CNRM-CM6–1	CMIP6	0.06	0.49	Small shift	Yes	4.8
CNRM-ESM2–1	CMIP6	0.13	1.85	Northward	Yes	4.8
CSIRO-Mk3–6-0	CMIP5	−0.11	0.98	Exclude		4.1
EC-Earth3	CMIP6	−0.02	−0.94	Southward	Yes	4.3
EC-Earth3-Veg	CMIP6	0.03	−0.77	Southward	Yes	4.3
FGOALS-f3-L	CMIP6	0.13	2.48	Northward	Yes	3
FGOALS-g3	CMIP6	0.28	5.83	Northward	Yes	2.9
FIO-ESM-2–0	CMIP6	−0.07	0.38	Small shift	Yes	
GFDL-CM3	CMIP5	0.03	−0.31	Small shift	Yes	4
GFDL-CM4	CMIP6	0.00	−0.24	Small shift	Yes	3.9
GFDL-ESM2G	CMIP5	0.19	1.74	Exclude		2.4
GFDL-ESM2M	CMIP5	0.07	0.80	Exclude		2.4
GFDL-ESM4	CMIP6	0.05	1.01	Northward	Yes	2.6
GISS-E2-H	CMIP5	−0.01	3.07	Exclude		2.3
GISS-E2-H-CC	CMIP5	−0.07	4.01	Exclude		
GISS-E2-R	CMIP5	0.11	4.60	Exclude		2.1
GISS-E2-R-CC	CMIP5	0.12	3.45	Exclude		
HadGEM2-AO	CMIP5	0.02	0.38	Small shift		
HadGEM2-CC	CMIP5	0.04	−0.66	Southward		
INM-CM4–8	CMIP6	0.01	2.30	Exclude		1.8
INM-CM5–0	CMIP6	0.03	−0.35	Exclude		1.9
INMCM4	CMIP5	0.00	−0.70	Exclude		2.1
IPSL-CM5A-LR	CMIP5	0.04	−1.29	Southward	Yes	4.1
IPSL-CM5A-MR	CMIP5	0.07	−1.53	Southward	Yes	4.03
IPSL-CM5B-LR	CMIP5	0.08	1.43	Northward	Yes	2.6
IPSL-CM6A-LR	CMIP6	−0.04	−1.50	Southward	Yes	4.6
KACE-1–0-G	CMIP6	−0.02	−0.35	Small shift	Yes	4.5
MIROC-ES2L	CMIP6	0.06	1.40	Northward	Yes	2.7
MIROC-ESM	CMIP5	−0.08	7.64	Exclude		4.7
MIROC-ESM-CHEM	CMIP5	0.11	10.74	Exclude		
MIROC5	CMIP5	−0.13	−2.55	Southward	Yes	2.7
MIROC6	CMIP6	−0.14	−3.31	Southward	Yes	2.6
MPI-ESM-LR	CMIP5	0.01	0.17	Exclude		3.6
MPI-ESM-MR	CMIP5	−0.02	0.14	Exclude		3.3
MPI-ESM1–2-HR	CMIP6	−0.03	−0.17	Small shift	Yes	3
MPI-ESM1–2-LR	CMIP6	−0.01	−0.63	Southward	Yes	3

TABLE A2. (*Continued*)

Model	MIP	Slope change (°N/°E)	Position change (°N)	Group	Moisture budget	ECS
MRI-CGCM3	CMIP5	−0.03	1.50	Northward	Yes	2.6
MRI-ESM1	CMIP5	−0.07	2.02	Northward		
NESM3	CMIP6	0.03	−0.98	Southward	Yes	4.8
NorESM1-M	CMIP5	0.01	−1.05	Southward	Yes	2.8
NorESM1-ME	CMIP5	0.03	−0.77	Southward		
NorESM2-MM	CMIP6	−0.07	−0.77	Southward	Yes	2.5
TaiESM1	CMIP6	−0.09	−1.15	Southward	Yes	4.4
UKESM1–0-LL	CMIP6	−0.15	−1.92	Southward	Yes	5.3

Environmental Science Programme's Earth Systems and Climate Change Hub and the Australian Research Council Centre of Excellence for Climate Extremes (Grant CE170100023). We acknowledge the World Climate Research Programme's Working Group on Coupled Modelling, which is responsible for CMIP, and we thank the climate modeling groups for producing and making available their model output. CMIP5 and CMIP6 model outputs were made available with the assistance of resources from the National Computational Infrastructure (NCI), which is supported by the Australian government. We would also like to thank two anonymous reviewers for their helpful and constructive comments.

Data availability statement. The model output and observational data are publicly available from https://cmip.llnl.gov/cmip5/data_portal.html, https://www.ncei.noaa.gov/data/global-precipitation-climatology-project-gpcp-monthly/, and https://www.metoffice.gov.uk/hadobs/hadisst/. Code is available on request from S.N.

APPENDIX

Model Evaluation and SPCZ Characteristics

Table A1 shows the model names and whether these are CMIP5 or CMIP6 models, the correlations and root-mean-square errors of model precipitation and temperature against observations over the SPCZ region, and the diagnosed model SPCZ slope and position (latitude).

Table A2 shows the change in model SPCZ slope and position in future climate relative to historical climate, the model "storyline" classification (northward, southward, or small shift), whether the model was used for moisture budget calculations, and the value of model equilibrium climate sensitivity.

REFERENCES

Adler, R. F., and Coauthors, 2003: The version-2 Global Precipitation Climatology Project (GPCP) Monthly Precipitation Analysis (1979–present). *J. Hydrometeor.*, **4**, 1147–1167, https://doi.org/10.1175/1525-7541(2003)004<1147:TVGPCP>2.0.CO;2.

Bishop, C. H., and G. Abramowitz, 2013: Climate model dependence and the replicate Earth paradigm. *Climate Dyn.*, **41**, 885–900, https://doi.org/10.1007/s00382-012-1610-y.

Brown, J. R., S. B. Power, F. P. Delage, R. A. Colman, A. F. Moise, and B. F. Murphy, 2011: Evaluation of the South Pacific convergence zone in IPCC AR4 climate model simulations of the twentieth century. *J. Climate*, **24**, 1565–1582, https://doi.org/10.1175/2010JCLI3942.1.

——, A. F. Moise, and F. P. Delage, 2012: Changes in the South Pacific Convergence Zone in IPCC AR4 future climate projections. *Climate Dyn.*, **39**, 1–19, https://doi.org/10.1007/s00382-011-1192-0.

——, ——, and R. A. Colman, 2013: The South Pacific Convergence Zone in CMIP5 simulations of historical and future climate. *Climate Dyn.*, **41**, 2179–2197, https://doi.org/10.1007/s00382-012-1591-x.

——, and Coauthors, 2020: South Pacific Convergence Zone dynamics, variability and impacts in a changing climate. *Nat. Rev. Earth Environ.*, **1**, 530–543, https://doi.org/10.1038/s43017-020-0078-2.

Cai, W., and Coauthors, 2012: More extreme swings of the South Pacific convergence zone due to greenhouse warming. *Nature*, **488**, 365–369, https://doi.org/10.1038/nature11358.

Chadwick, R., P. Good, T. Andrews, and G. Martin, 2014: Surface warming patterns drive tropical rainfall pattern responses to CO_2 forcing on all timescales. *Geophys. Res. Lett.*, **41**, 610–615, https://doi.org/10.1002/2013GL058504.

Chou, C., and J. D. Neelin, 2004: Mechanisms of global warming impacts on regional tropical precipitation. *J. Climate*, **17**, 2688–2701, https://doi.org/10.1175/1520-0442(2004)017<2688:MOGWIO>2.0.CO;2.

——, ——, C. A. Chen, and J. Y. Tu, 2009: Evaluating the "rich-get-richer" mechanism in tropical precipitation change under global warming. *J. Climate*, **22**, 1982–2005, https://doi.org/10.1175/2008JCLI2471.1.

Christensen, J. H., and Coauthors, 2013: Climate phenomena and their relevance for future regional climate change. *Climate Change 2013: The Physical Science Basis*, T. F. Stocker et al., Eds., Cambridge University Press, 1217–1308.

Chung, C. T. Y., and S. B. Power, 2015: Modelled rainfall response to strong El Niño sea surface temperature anomalies in the tropical Pacific. *J. Climate*, **28**, 3133–3151, https://doi.org/10.1175/JCLI-D-14-00610.1.

——, and ——, 2016: Modelled impact of global warming on ENSO-driven precipitation changes in the tropical Pacific. *Climate Dyn.*, **47**, 1303–1323, https://doi.org/10.1007/s00382-015-2902-9.

——, ——, J. M. Arblaster, H. A. Rashid, and G. L. Roff, 2014: Nonlinear precipitation response to El Niño and global warming in the Indo-Pacific. *Climate Dyn.*, **42**, 1837–1856, https://doi.org/10.1007/s00382-013-1892-8.

Dong, Y., K. C. Armour, M. D. Zelinka, C. Proistosescu, D. S. Battisti, C. Zhou, and T. Andrews, 2020: Intermodel spread in the pattern effect and its contribution to climate sensitivity in CMIP5 and CMIP6 models. *J. Climate*, **33**, 7755–7775, https://doi.org/10.1175/JCLI-D-19-1011.1.

Dutheil, C., and Coauthors, 2019: Impact of surface temperature biases on climate change projections of the South Pacific Convergence Zone. *Climate Dyn.*, **53**, 3197–3219, https://doi.org/10.1007/s00382-019-04692-6.

Evans, J. P., K. Bormann, J. Katzfey, S. Dean, and R. Arritt, 2016: Regional climate model projections of the South Pacific Convergence Zone. *Climate Dyn.*, **47**, 817–829, https://doi.org/10.1007/s00382-015-2873-x.

Eyring, V., S. Bony, G. A. Meehl, C. A. Senior, B. Stevens, R. J. Stouffer, and K. E. Taylor, 2016: Overview of the Coupled Model Intercomparison Project Phase 6 (CMIP6) experimental design and organization. *Geosci. Model Dev.*, **9**, 1937–1958, https://doi.org/10.5194/gmd-9-1937-2016.

Fiedler, S., and Coauthors, 2020: Simulated tropical precipitation assessed across three major phases of the Coupled Model Intercomparison Project (CMIP). *Mon. Wea. Rev.*, **148**, 3653–3680, https://doi.org/10.1175/MWR-D-19-0404.1.

Folland, C. K., J. A. Renwick, M. J. Salinger, and A. B. Mullan, 2002: Relative influences of the interdecadal Pacific oscillation and ENSO on the South Pacific convergence zone. *Geophys. Res. Lett.*, **29**, 1643, https://doi.org/10.1029/2001GL014201.

Grose, M. R., J. Bhend, S. Narsey, A. Sen Gupta, and J. R. Brown, 2014: Can we constrain CMIP5 rainfall projections in the tropical Pacific based on surface warming patterns? *J. Climate*, **27**, 9123–9138, https://doi.org/10.1175/JCLI-D-14-00190.1.

——, and Coauthors, 2020: Insights from CMIP6 for Australia's future climate. *Earth's Future*, **8**, e2019EF001469, https://doi.org/10.1029/2019EF001469.

Hawkins, E., and R. Sutton, 2009: The potential to narrow uncertainty in regional climate predictions. *Bull. Amer. Meteor. Soc.*, **90**, 1095–1108, https://doi.org/10.1175/2009BAMS2607.1.

——, and ——, 2011: The potential to narrow uncertainty in projections of regional precipitation change. *Climate Dyn.*, **37**, 407–418, https://doi.org/10.1007/s00382-010-0810-6.

Held, I. M., and B. J. Soden, 2006: Robust responses of the hydrological cycle to global warming. *J. Climate*, **19**, 5686–5699, https://doi.org/10.1175/JCLI3990.1.

Herger, N., G. Abramowitz, R. Knutti, O. Angélil, K. Lehmann, and B. M. Sanderson, 2018: Selecting a climate model subset to optimise key ensemble properties. *Earth Syst. Dyn.*, **9**, 135–151, https://doi.org/10.5194/esd-9-135-2018.

Jourdain, N. C., P. Marchesiello, C. E. Menkès, J. Lefèvre, E. M. Vincent, M. Lengaigne, and F. Chauvin, 2011: Mesoscale simulation of tropical cyclones in the South Pacific: Climatology and interannual variability. *J. Climate*, **24**, 3–25, https://doi.org/10.1175/2010JCLI3559.1.

Kiladis, G. N., H. von Storch, and H. Loon, 1989: Origin of the South Pacific convergence zone. *J. Climate*, **2**, 1185–1195, https://doi.org/10.1175/1520-0442(1989)002<1185:OOTSPC>2.0.CO;2.

Li, G., and S.-P. Xie, 2014: Tropical biases in CMIP5 multimodel ensemble: The excessive equatorial Pacific cold tongue and double ITCZ problems. *J. Climate*, **27**, 1765–1780, https://doi.org/10.1175/JCLI-D-13-00337.1.

Meehl, G. A., C. Covey, T. Delworth, M. Latif, B. McAvaney, J. F. B. Mitchell, R. J. Stouffer, and K. E. Taylor, 2007: The WCRP CMIP3 multi-model dataset: A new era in climate change research. *Bull. Amer. Meteor. Soc.*, **88**, 1383–1394, https://doi.org/10.1175/BAMS-88-9-1383.

——, C. A. Senior, V. Eyring, G. Flato, J. F Lamarque, R. J. Stouffer, K. E. Taylor, and M. Schlund, 2020: Context for interpreting equilibrium climate sensitivity and transient climate response from the CMIP6 Earth system models. *Sci. Adv.*, **6**, eaba1981, https://doi.org/10.1126/sciadv.aba1981.

Menkes, C. E., M. Lengaigne, P. Marchesiello, N. C. Jourdain, E. M. Vincent, J. Lefèvre, F. Chauvin, and J.-F. Royer, 2012: Comparison of tropical cyclogenesis indices on seasonal to interannual timescales. *Climate Dyn.*, **38**, 301–321, https://doi.org/10.1007/s00382-011-1126-x.

Möbis, B., and B. Stevens, 2012: Factors controlling the position of the Intertropical Convergence Zone on an aquaplanet. *J. Adv. Model. Earth Syst.*, **4**, M00A04, https://doi.org/10.1029/2012MS000199.

National Research Council, 1979: *Carbon Dioxide and Climate*: A *Scientific Assessment*. National Academies Press, 34 pp., https://doi.org/10.17226/12181.

Nguyen, K. C., J. J. Katzfey, and J. L. McGregor, 2012: Global 60 km simulations with CCAM: Evaluation over the tropics. *Climate Dyn.*, **39**, 637–654, https://doi.org/10.1007/s00382-011-1197-8.

Niznik, M. J., B. R. Lintner, A. J. Matthews, and M. J. Widlansky, 2015: The role of tropical–extratropical interaction and synoptic variability in maintaining the South Pacific convergence zone in CMIP5 models. *J. Climate*, **28**, 3353–3374, https://doi.org/10.1175/JCLI-D-14-00527.1.

Ramsay, H. A., and A. H. Sobel, 2011: Effects of relative and absolute sea surface temperature on tropical cyclone potential intensity using a single-column model. *J. Climate*, **24**, 183–193, https://doi.org/10.1175/2010JCLI3690.1.

Rayner, N. A., D. E. Parker, E. B. Horton, C. K. Folland, L. V. Alexander, D. P. Rowell, E. C. Kent, and A. Kaplan, 2003: Global analyses of sea surface temperature, sea ice, and night marine air temperature since the late nineteenth century. *J. Geophys. Res. Atmos.*, **108**, 4407, https://doi.org/10.1029/2002JD002670.

Samanta, D., K. B. Karnauskas, and N. F. Goodkin, 2019: Tropical Pacific SST and ITCZ biases in climate models: Double trouble for future rainfall projections? *Geophys. Res. Lett.*, **46**, 2242–2252, https://doi.org/10.1029/2018GL081363.

Seager, R., N. Naik, and G. A. Vecchi, 2010: Thermodynamic and dynamic mechanisms for large-scale changes in the hydrological cycle in response to global warming. *J. Climate*, **23**, 4651–4668, https://doi.org/10.1175/2010JCLI3655.1.

Shepherd, T. G., and Coauthors, 2018: Storylines: An alternative approach to representing uncertainty in physical aspects of climate change. *Climatic Change*, **151**, 555–571, https://doi.org/10.1007/s10584-018-2317-9.

Takahashi, K., and D. S. Battisti, 2007: Processes controlling the mean tropical Pacific precipitation pattern. Part II: The SPCZ and the southeast Pacific dry zone. *J. Climate*, **20**, 5696–5706, https://doi.org/10.1175/2007JCLI1656.1.

Taylor, K. E., R. J. Stouffer, and G. A. Meehl, 2012: An overview of CMIP5 and the experiment design. *Bull. Amer. Meteor. Soc.*, **93**, 485–498, https://doi.org/10.1175/BAMS-D-11-00094.1.

Tian, B., 2015: Spread of model climate sensitivity linked to double-Intertropical Convergence Zone bias. *Geophys. Res. Lett.*, **42**, 4133–4141, https://doi.org/10.1002/2015GL064119.

van Oldenborgh, G. J., H. Hendon, T. Stockdale, M. L'Heureux, E. C. De Perez, R. Singh, and M. Van Aalst, 2021: Defining

El Niño indices in a warming climate. *Environ. Res. Lett.*, **16**, 044003, https://doi.org/10.1088/1748-9326/abe9ed.

Vincent, D. G., 1994: The South Pacific convergence zone (SPCZ): A review. *Mon. Wea. Rev.*, **122**, 1949–1970, https://doi.org/10.1175/1520-0493(1994)122<1949:TSPCZA>2.0.CO;2.

Vincent, E. M., M. Lengaigne, C. E. Menkes, N. C. Jourdain, P. Marchesiello, and G. Madec, 2011: Interannual variability of the South Pacific Convergence Zone and implications for tropical cyclone genesis. *Climate Dyn.*, **36**, 1881–1896, https://doi.org/10.1007/s00382-009-0716-3.

Widlansky, M. J., P. J. Webster, and C. D. Hoyos, 2011: On the location and orientation of the South Pacific Convergence Zone. *Climate Dyn.*, **36**, 561–578, https://doi.org/10.1007/s00382-010-0871-6.

——, A. Timmermann, K. Stein, S. McGregor, N. Schneider, M. H. England, M. Lengaigne, and W. Cai, 2013: Changes in South Pacific rainfall bands in a warming climate. *Nat. Climate Change*, **3**, 417–423, https://doi.org/10.1038/nclimate1726.

Xie, P., and P. A. Arkin, 1997: Global precipitation: A 17-year monthly analysis based on gauge observations, satellite estimates, and numerical model outputs. *Bull. Amer. Meteor. Soc.*, **78**, 2539–2558, https://doi.org/10.1175/1520-0477(1997)078<2539:GPAYMA>2.0.CO;2.

Zelinka, M. D., T. A. Myers, D. T. McCoy, S. Po-Chedley, P. M. Caldwell, P. Ceppi, S. A. Klein, and K. E. Taylor, 2020: Causes of higher climate sensitivity in CMIP6 models. *Geophys. Res. Lett.*, **47**, e2019GL085782, https://doi.org/10.1029/2019GL085782.

Zhou, W., S.-P. Xie, and D. Yang, 2019: Enhanced equatorial warming causes deep-tropical contraction and subtropical monsoon shift. *Nat. Climate Change*, **9**, 834–839, https://doi.org/10.1038/s41558-019-0603-9.